Southern Methodist University

SMU Scholar

Spring 5-11-2024

SCREEN FOR BENEFICIAL GENETIC AND CHEMICAL MODIFIERS IN DROSOPHILA MODELS OF ALS AND TRAUMATIC BRAIN INJURY

Will Bonderer
Southern Methodist University, wbonderer@smu.edu

Follow this and additional works at: https://scholar.smu.edu/hum_sci_biologicalsciences_etds

Part of the Biology Commons, Genetics Commons, and the Molecular and Cellular Neuroscience Commons

Biological Sciences Theses and Dissertations   Biological Sciences

Spring 5-11-2024

SCREEN FOR BENEFICIAL GENETIC AND CHEMICAL MODIFIERS IN DROSOPHILA MODELS OF ALS AND TRAUMATIC BRAIN INJURY

Will Bonderer

SCREEN FOR BENEFICIAL GENETIC AND CHEMICAL MODIFIERS IN *DROSOPHILA*

MODELS OF ALS AND TRAUMATIC BRAIN INJURY

Approved by:

_____
Dr. Adam D. Norris, Ph.D.
Assistant Professor of Biological Sciences, SMU
Assistant Professor of Biochemistry, UCR

_____
Dr. Richard Jones, Ph.D.
Professor of Biological Sciences, SMU

_____
Dr. Zhihao Wu, Ph.D.
Assistant Professor of Biological Sciences, SMU

SCREEN FOR BENEFICIAL GENETIC MODIFIERS IN *DROSOPHILA* MODELS OF

ALS AND TRAUMATIC BRAIN INJURY

A Thesis Presented to the Graduate Faculty of the

Dedman College

Southern Methodist University

in

Partial Fulfillment of the Requirements

for the degree of

Master of Science

in

Molecular and Cellular in Biology

by

Will Bonderer

B.A., Biological Sciences, Southern Methodist University

May 11, 2024

ACKNOWLEDGMENTS

I would first like to thank my advisor and mentor, Dr. Zhihao Wu, who has guided and supported me in my research since I was an undergraduate student. Thank you for giving me countless opportunities, pushing me in my studies and research, and being both an exemplary scientist and person. This work would not have been accomplished without Dr. Wu or the help of my fellow lab members, Foozhan, Yinglu, Adaeze, Ting, Yuanna, Bei, and Jessi. I could not have asked for a more positive and productive experience in the lab. I would also like to thank my committee members, Dr. Richard Jones and Dr. Adam Norris, for their continued guidance and questions that challenged me as a graduate student. I especially thank Judith Benes for her constant guidance, empathy, and support during my years in the fly lab.

I would like to express my deepest gratitude to my parents, Tiana and Michael, for providing me the opportunity to further my education and embrace experiences I never thought I would have. I cannot thank you enough for your love and constant support. Thank you to my friends and Emily for always being there through the ups and downs and believing in me.

Bonderer, Will   B.A., Biological Sciences, Southern Methodist University

<u>Screen for Beneficial Genetic and Chemical Modifiers in *Drosophila* Models
of ALS and Traumatic Brain Injury</u>

Advisor: Professor Zhihao Wu

Master of Science conferred May 11, 2024

Thesis completed May 3, 2024

The underlying molecular processes of aberrant protein expression in neurodegeneration are intricate and multifaceted, with ribosome-associated quality control (RQC) emerging as a promising avenue of exploration. Ribosome-associated quality control is integral to cellular function. Its evolutionarily conserved pathway encompasses a network of mechanisms designed to ensure the fidelity of protein synthesis, folding, and degradation within the cells of all eukaryotes. The ribosome, central to protein synthesis, plays a pivotal role in this quality control network, and its malfunction can lead to the accumulation of misfolded or aberrant proteins. In the context of neurodegenerative disorders, this dysfunction can have dire consequences. Protein misfolding and aggregation are common features in neurodegenerative diseases, and ribosome-associated quality control is critical in preventing or mitigating these events. Therefore, dysfunction in ribosome-associated quality control mechanisms is not merely a consequence of neurodegenerative disorders; it may also be a driving force, creating a feedback loop that exacerbates protein homeostasis failure.

This study aims to investigate the potential role of ribosome-associated quality control in *Drosophila* models in the context of neurodegenerative diseases and cellular stress. In Chapter 1, we established a protocol for the construction of a high-throughput method to induce traumatic

brain injury in *D. Melanogaster*. In Chapter 2, we investigated the role of TDP-43 ribonuclear protein in the rescue of mitochondrial morphology in *PINK1* mutant models. Chapter 3 aims to determine the effects of Usp10/USP10 and rin/G3BP1 overexpression and knockdown under drug-induced proteotoxic stress in aged flies. Finally, the appendix focuses on establishing baseline lifespan and histological data in transgenic fruit fly models of Batten Disease for future screenings of quality control proteins.

TABLE OF CONTENTS

Dedicated to the fruit flies that have sacrificed their lives for my research.

SPECIFIC AIMS

Chapter 1: Establish a protocol for the construction of a precise and high throughput method to induce TBI in _D. Melanogaster_

The Bonini lab at the University of Pennsylvania created the first design and protocol for

the induction of dTBI using the piezoelectric actuator[1]. Although the piezoelectric actuator

outlined in the original protocol produces identical compression as the device outlined in our

protocol, the circuit design and central components have been modified. For example, the

voltage booster is an integral component of the original protocol; however, the discontinuation of

this part by the manufacturer disrupts the original design and creates a need for replacement and

circuit modifications. These modifications include replacements to the power source, digital

display, potentiometer, SPST relay, structural components, and the elimination of the buck

converter. The construction and calibration of this device provide a high throughput method to

screen conserved genetic modifiers of TBI and induce cellular stress in fly models of

neurodegeneration.

Chapter 2: Hydrogen Gas Pink1 Mediated Rescue Of Mitochondrial Morphology In Muscle Tissue

Hydrogen gas may alleviate neurotoxicity and cellular damage from reactive oxygen

species (ROS). When the _Drosophila_ PINK1 homolog _pivi_ is knocked down and crossed with

wild-type or mutant TDP-43, a rescue in mitochondrial morphology is observed. I aim to

characterize mitochondrial morphology in Drosophila muscle cells and create a research plan for

further investigation of the interaction between TDP-43, hydrogen treatment, and PINK1.

Chapter 3: Determine the effects of *Usp10*/USP10 and *rin*/G3BP1 overexpression and knockdown under drug-induced proteotoxic stress in aged flies

Usp10 and *rin* are integral proteins in the 40S ribosomal subunit recycling complex. Our lab has shown that disrupting these proteins has deleterious effects on protein translation, mitochondrial homeostasis, and the regulation of mTOR pathways. This work aims to assist our lab's Ph.D. candidate in investigating the link between mitochondrial quality control and ribosome-associated quality control under aging and toxic stress conditions.

CHAPTER 1

PROTOCOL FOR THE CONSTRUCTION OF THE PIEZOELECTRIC ACTUATOR

1.1 Abstract

Traumatic brain injury (TBI) is a global health concern, occurring at an alarming rate of approximately 50 million new cases annually and standing as the foremost cause of injury-related fatalities[2]. Defined broadly, TBI is the result of an external force to the head ranging from a mild blow from combat or contact sports, bump or crash, blast wave, or penetration from a projectile. In addition to the debilitating effects associated with the primary injury to the head, the secondary, cascading effects of TBI are neurotoxic and correlated with a myriad of long-term neurodegenerative diseases such as Chronic Traumatic Encephalopathy (CTE), Alzheimer's disease (AD), dementia pugilistica (DP), Amyotrophic lateral sclerosis (ALS), and post-traumatic epilepsy. *Drosophila melanogaster* (fruit fly or fly) is a versatile model organism that has significantly contributed to our understanding of neurological diseases. Due to its substantial genetic similarity to humans and short lifespan, *Drosophila* provides an invaluable *in vivo* model to study how traumatic brain injury (TBI) might manifest in an aging brain. Importantly, when subjected to impact, flies exhibit behaviors characteristic of mammalian models, including severity-dependent ataxia, reduced lifespan, and neurodegeneration[3]. Using the piezoelectric actuator device to induce TBI in *Drosophila* establishes an injury model that accurately mirrors crucial pathophysiological aspects observed in mammalian traumatic brain injuries, paving the way for identifying vital molecular mechanisms essential for future therapeutic advancements.

1.2 Background

It is well known that primary neural injury is a result of acceleration forces that harm cellular architecture, like axons, glia, and blood vessels[4]. When the primary mechanical damage breaches the blood-brain barrier (BBB), it leads to dysregulated polarization of cellular membranes and glutamate excitotoxicity, ultimately causing an excessive buildup of intracellular calcium[5]. Calcium overload across synapses may culminate in cell death through secondary molecular events such as oxidative stress, inflammation, and mitochondrial dysfunction[6,7]. Notably, neurodegenerative diseases like chronic traumatic encephalopathy (CTE), dementia pugilistica (DP), Amyotrophic lateral sclerosis (ALS), and post-traumatic epilepsy all share in these deleterious secondary pathways[8,9]. TBI has been implicated in the acceleration and exacerbation of neurodegenerative and aging phenotypes, but further investigation is needed to reveal the underlying mechanisms and extent to which TBI is involved[9].

Drosophila melanogaster has played a pivotal role in elucidating mechanisms of biological processes with direct relevance to human disease, including neurodegenerative disorders[10]. Its easily manipulated genome and precise expression of target genes using the *UAS-Gal4* system enables traceability of cellular and molecular changes[10]. Furthermore, its high reproducibility and shortened lifespan provides an ideal model to study aging. While aging and many forms of neurodegeneration are commonly modeled in *Drosophila,* the study of TBI in this small organism has proved challenging.

A novel method developed by the Bonini lab (University of Pennsylvania) uses a piezoelectric actuator to model the impact of a TBI on the head of *Drosophila*[1]. The method is automated and high-throughput – allowing for the testing of up to 10 flies at the same force of compression. The level of head compression is a key determinant of brain injury severity,

4

offering distinct injury thresholds: mild, moderate, and severe. In this way, the heterogeneity of brain injury can be controlled[1].

1.3 Materials

Fly Stock

- *w1118* flies (Bloomington Stock #5905)

Equipment for assembly of dTBI controller circuit

A. Power supply (amazon.com ASIN #B07KR392XQ)

B. Potentiometer (amazon.com ASIN #B0BZ765TR3)

C. 5VDC SPDT relay (amazon.com ASIN #B09M9P23BS)

D. Digital voltmeter display (amazon.com ASIN #B072BY4XZ7)

E. Arduino microcontroller (digikey.com #1050-1024-ND; Arduino #A000066)

F. Pushbutton (amazon.com ASIN #B0772KYPPM; Ocrtech)

G. Proportional voltage booster (amazon.com ASIN #B08B63RYD6)

H. Electrical terminal connector (amazon.com ASIN #B01A6LTK44; MUYI
    #5xSKUMY20973)

I.   Non-Insulated Block Spade Terminal (Vetco Electronics #SR-SPA-1N),

J.   Polycarbonate sheet (McMaster Carr #8574K321)

K. Piezoelectric actuator (piezo.com, low-throughput setup #Q220-A4-203YB

Other electrical equipment

L. Breadboard (CircuitSpecialists #WB-801)

M. Solderable breadboard (digikey.com #1568-1082-ND; SparkFun Electronics #12070)

N. 10K Ohm resistor (amazon.com ASIN #B07QJB31M7)

O. Helping hands soldering tool (amazon.com ASIN #B00GIKVP5K; Alphidia QuadHands® Classic Helping Hands)

P. M2.5 Nylon Hex Standoff Female (amazon.com ASIN #B07DCNZSRD; Albert Guy)

Q. Mounting screws 4-40 (McMaster Carr #92196A108)

R. Electrical wire strippers (McMaster Carr #7294K14)

S. Digital multimeter (amazon.com ASIN #B01N9QW620; Etekcity #MSR-R500)

T. Soldering kit (amazon.com ASIN #B06XZ31W3M; Anbes #GJM001-US)

U. 22 gauge wire (amazon.com ASIN # B00B4ZQ3L0; RSR Electronics Inc #27WK22STR25)

Equipment for fly work

V. Standard fly food vials

W. Classic Heisenberg collar: design specification (https://aktivnetz.de/universitaet/filab/Atlas/pics/atlas/collar.gif), Genesee Scientific #48-100

X. Platform (See software for CAD model)

Y. Mirror Wedge (See software for CAD model)

Z. Box and Lid (See software for CAD model)

Software

- Camera on Z16 APO (Leica DFC420)

- Leica Acquire Application

- Mirror – needs to be cut to size with a holder so it rests stably at a 45° angle (McMaster Carr #1017T316)

- Arduino IDE (https://www.arduino.cc)

- dTBI Arduino code[1] (box.com)

- CAD Models for 3d Print (box.com)

1.4 Procedure

Wiring the input power supply (Steps 1-5)

1. Start by creating a working prototype of the circuit using a solderless breadboard. Once the circuit is working, the wires with header pins should be soldered onto a solderless breadboard. The voltage booster **(G)** will be the central power supply for the piezoelectric. Unscrew the IN (+) terminal and connect a red 22 gauge wire. Connect the other side of the wire to the Arduino **(E)** Vin pin.

2. Ground the voltage booster and the Arduino microcontroller by unscrewing IN (-) terminal of voltage booster and connecting a black 22 gauge wire. Connect the other side of the wire to the "GND" pin.

3. This design will only require one breadboard **(L)**. Connect another 22 gauge black wire to the IN (-) terminal of the voltage booster **(G)**. Insert the other side of the wire anywhere on the (-) rail of the breadboard rail **(L)**.

4. Connect the SPST relay switch **(C)** to the breadboard shown in figure x. The relay consists of 5 pins. The pins should be placed on the breadboard holes E8, G8 G13, E12, E14.

5. Connect a black 22-gauge wire from the (-) rail of the breadboard to hole C8. Next, connect a blue 22 gauge wire from hole H8 to the Arduino **(E)** pin 13. This wire will supply a voltage pulse from the Arduino to the switch.

Wiring the pushbutton (Steps 6-10)

6. The button **(F)** will have four legs total; 2 pairs of legs directly adjacent to one another. Using a multimeter on the resistance setting (~), place the red and black probes on opposite sides until the multimeter beeps or displays 0V. These are opposite sides of the push button.

7. Strip (the wire strippers **S**) and cut one end of a blue 22-gauge wire with header pins. Wrap the copper around one leg of the pushbutton and solder **(F)**. Connect the other end of the blue wire to pin 7 of the Arduino **(E)**.

8. Repeat the previous step using a grey 22 gauge wire on the opposite side leg of the pushbutton **(F)**. Connect the other end of the grey wire to the GND pin of the Arduino **(E)**.

9. Add a black 22-gauge wire without header pins around a leg on the same side of the wire in step 8. This pushbutton will need a resistor, so take a 10k Ohm resistor **(N)** and solder one end to the open end of the black wire.

10. Cut and strip one end of a second, black 22-gauge wire with header pins, leaving the header pin on the other end intact. Solder the exposed portion of the wire to the 10k Ohm resistor **(N)**. Add an additional layer of conductive tape around the soldered connection to cover any exposed wire. Connect the end of the wire with a header pin to the Arduino's 5V pin **(E)**.

Mounting the piezo transducer (Steps 11-12)

11. The piezo will need to be mounted about an inch off of the polycarbonate sheet (**J**). Measure this distance and mark the location of the piezo's two holes on the polycarbonate (**J**).

12. Drill two holes through the marked points with a .0890 bit. Tap the holes and mount the piezo (**K**) with size 4-40 threaded screws (**R**).

Checkpoint (Steps 13-24)

13. This is also a good point to check if the Arduino, button, and voltage booster are wired correctly. CAUTION: when active, the voltage booster can supply up to 100V. DO NOT TOUCH the <u>output terminals</u> or the <u>magnetic coil/capacitors</u> when the power is connected. Before connecting the barrel plug of power supply (**A**) to the voltage booster, disconnect the power adaptor (power brick) from the power chord. It is safest to connect the DC current from the wall socket to the power adaptor than from the barrel plug to the voltage booster.

14. If wired correctly, the Arduino should be powered by the voltage booster, indicated by a green light.

15. To upload code to the Arduino, connect it to a computer with Arduino IDE installed. Once running, select the Arduino board from the dropdown menu, paste, and upload the code.

16. With this code installed on the Arduino, the pushbutton will be functional. When the button is pressed, the TX LED light should blink on and off, indicating a 5V pulse is being supplied from the Arduino to the relay switch.

17. Using a multimeter on the voltage setting, attach the red probe to the IN (+) terminal of the voltage booster and the black probe to the IN (-) terminal of the voltage booster. The multimeter should read 12V.

18. Repeat the previous step on the OUT (+ and -) terminals of the voltage booster to gauge its voltage output. For wiring purposes, the voltage should be <20V. If it is greater than 20V, use a Philips head screwdriver and turn the brass knob atop the blue potentiometer on the voltage booster marked "V-ADJ" to the left until the multimeter reads <20V.

Wiring the output voltage (Steps 19-24)

19. With the piezo mounted, it is now ready to be connected to the voltage booster (**G**) and SPST relay (**C**). Make sure the power supply is not plugged in for these steps.

20. Connect the male and female ends of the terminal connectors (**H**). Next, cut and strip one end of a red, 22-gauge wire with header pins long enough to reach the breadboard safely. Solder this end to the red wire of the terminal connector. Connect the end of the wire with the header pin to hole H13 on the breadboard (**C**) adjacent to the relay pin. This wire will high voltage from the voltage booster to the relay.

21. Cut and strip both ends of a black, 22-gauge wire without header pins long enough to reach the piezo's black wire. Solder one end of this wire to the black wire of the terminal connector (**H**) and the other end to the small, black wire of the piezo (**K**). Wrap any exposed copper with conductive tape. This wire will ground the piezo to the voltage booster.

22. Unscrew the OUT (+) terminal of the voltage booster (**G**) and attach the red wire from the terminal connect (**H**). Likewise, unscrew the OUT (-) terminal of the voltage booster and attach the black wire from the terminal connector.

23. Finally, cut and strip one end of a red, 22-gauge gauge wire with header pins long enough to connect the SPST relay and the red wire of the piezo. Solder the stripped end of the wire to the small red wire of the piezo **(K).** Wrap any exposed copper with conductive tape. Connect the end of the wire with the header pin to hole C12 on the breadboard **(C).** This wire will supply high voltage to the piezo from the relay switch.

24. The circuit is complete. When power is supplied, the piezo should only move when the button is pressed. When the button is pressed, there will be two clicking sounds, one from the magnetic switch of the SPST relay and another from the bending of the piezo transducer.

Wiring the potentiometer (Steps 25-29)

25. Once the voltage booster is inside the enclosure, it can be difficult to adjust its output voltage level using a screwdriver and read the voltage without a multimeter. The voltage level can be easily adjusted using a potentiometer mounted and digital display mounted atop the enclosure. Start by unscrewing the four screws that secure the voltage booster to the metal heat sink. Place the voltage booster in the helping hands tool to clip and hold the circuit board in place. Locate the blue potentiometer from step 18 and identify the three pins on the underside of the board that hold it in place. Set the soldering iron to a high temperature and melt the solder. The metal will re-solidify quickly, so the solder must be removed with the de-soldering pump while it is still hot. The potentiometer may be removed using pliers.

26. Once the blue potentiometer has been removed, three pins should be exposed. Cut and strip three wires, each about three inches long. The wires are red, black, and white in color. Wrap the copper from each wire along the three holes of the 100k ohm

potentiometer **(B)** and solder. The order of the wires from right to left should be red, white, and black. Solder the ends of these wires to the three, exposed pins on the potentiometer, starting with the black wire corresponding to the pin closest to the edge of the board. The white wire will be the middle pin, and the red wire will be the top pin.

Mounting inside of the enclosure

27. The enclosure in this protocol and its exact dimensions are 3D printed using the files attached. Drill holes on the sides of the enclosure so that the terminal connectors and power supply can be fitted through. Additionally, a hole should be drilled into the lid of the enclosure so that the knob of the potentiometer may be secured.

28. Using the hex standoffs **(Q),** mount the breadboard and Arduino and place them inside the enclosure.

Calibration

Generation of voltage vs. displacement graph (excerpt from original protocol[1])

29. "The dTBI device should be calibrated under Z16 APO (Leica DFC420) microscope. To visualize the camera live stream and record videos to Mac or PC, download Leica Acquire.

31. Place an empty collar atop the platform **(X)** and underneath the piezoelectric **(K)**. Move the 45°-angled mirror up against it to view the empty fly collar. Mark the spot on the microscope stand where the mirror and piezo is located to ensure the angle is consistent.

32. "Adjust the brightness, zoom and focus to capture the reflection of the piezoelectric in the angled mirror".

33. "Using a frame rate of at least 10 fps, capture 3 replicate videos of the piezoelectric deflection events in 5V steps, starting from 35V till 80V".

34. Analyze the videos in ImageJ, using the Manual Tracking plugin to track a single pixel on corner of the piezoelectric to measure the y-displacement.

35. Generate a graph between voltage and y-displacement to ensure that the piezoelectric responds linearly to the voltage (see Anticipated Results)."[1]

1.5 Discussion

The piezoelectric actuator device that can induce traumatic brain injury in an *in vivo* aging and disease model. Unlike previous dTBI devices, the piezo produces a direct impact on the fly head and is most comparable to controlled cortical impact (CCI) or fluid percussion models in murine or rodent models. *Drosophila* has several advantages over mouse or rodent models, such as a rapid generation time, low genetic variability, and low cost, which allow for large-scale screenings of gene targets. Additionally, Drosophila is an ideal model to study the long-term effects and mechanisms of TBI because of its conserved genetic makeup and short lifespan. Crucially, Drosophila displays similar symptoms to humans after a head injury, including ataxia, disorganized movement, disrupted circadian rhythm, and gastrointestinal defects.

Autopsy reports have shown correlations between a history of TBI and protein deposition in the human brain.[4] Among the brains classified as stage IV CTE and prolonged history of repeated head trauma, 52 (91%) cases were found to have amyloid-β deposition. Deposition of TDP-43 and α-synuclein were found in all stages of CTE pathology; TDP-43 deposition occurred in 47 (83%) and α-synuclein deposition occurred in 23 (40%) stage IV CTE cases.[4]

Recent studies of dTBI on TDP-43 mutant models have also revealed a correlation between TBI and the accumulation of insoluble, ubiquitinated TDP-43 protein, along with stress

granule formation of r*in*/GB3P1.[11] Although their data is relevant and informative to the focus of our lab, I believe their data are limited by the spring-based induction of dTBI. Their findings may be even more pronounced if repeated using the piezo.

Other molecular events in TBI include oxidative stress and a sustained imbalance of reactive oxygen species and proteosomal dysfunction include Hsp70 chaperone activity.[3] Hydrogen gas is found to act as an antioxidant, and a decrease may alleviate some of the detrimental effects of TBI-induced ROS in a TDP-43 mutant model, as I find in Chapter 2.

Additionally, a number of RQC genes should be tested using the piezo. After induction of head trauma, fly samples can be collected at multiple different time points and western blot should be performed for detection in protein changes. Ref2p and Rin antibodies may be used as markers for the presence of autophagy and stress granule formation during proteotoxic stress. If a rescue is seen in any these phenotypes and protein markers, RQC may be implicated in the pathogenesis of TBI.
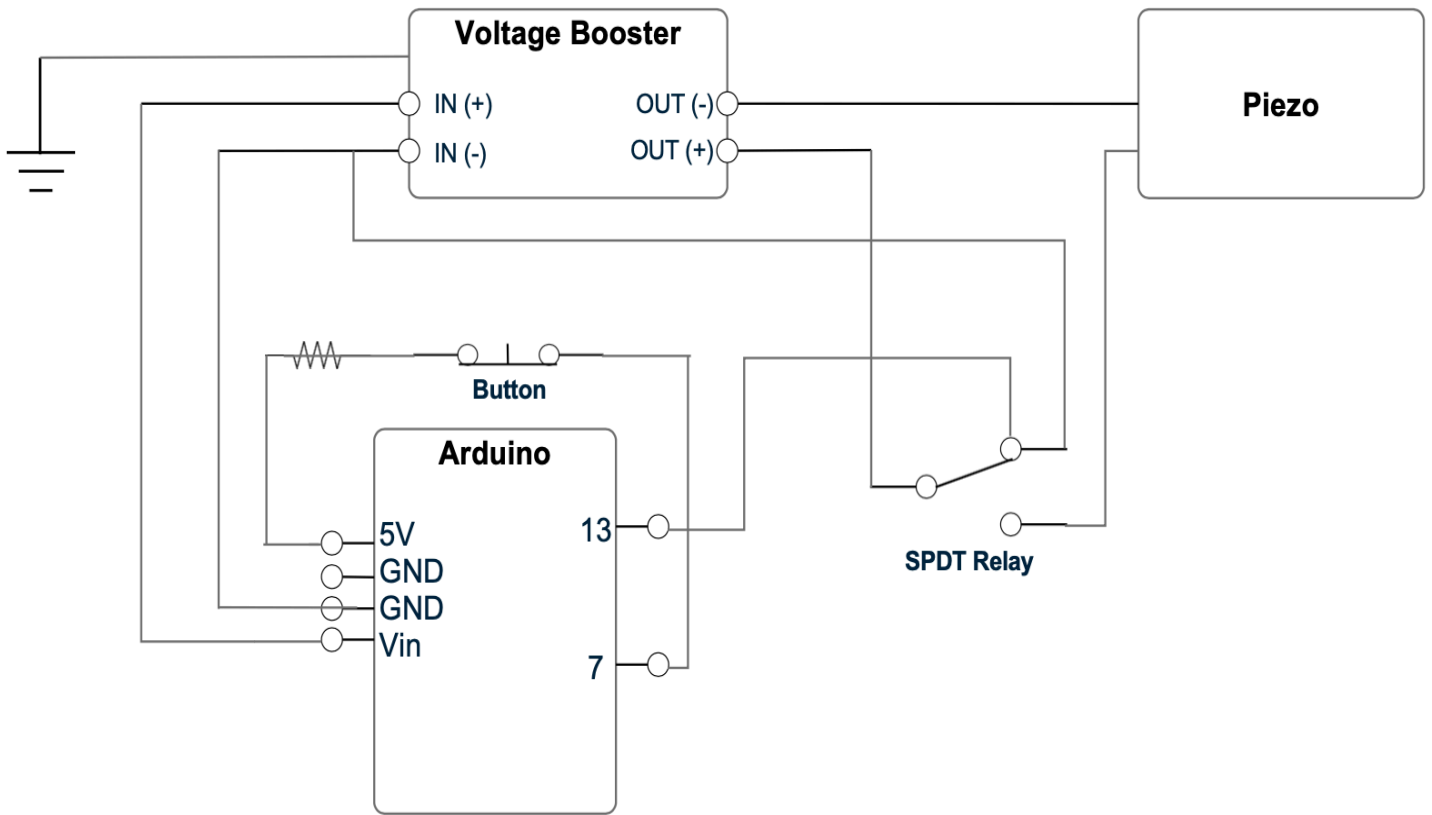
Figure 1-1 Wiring Diagram of the piezoelectric actuator (Wu Lab)
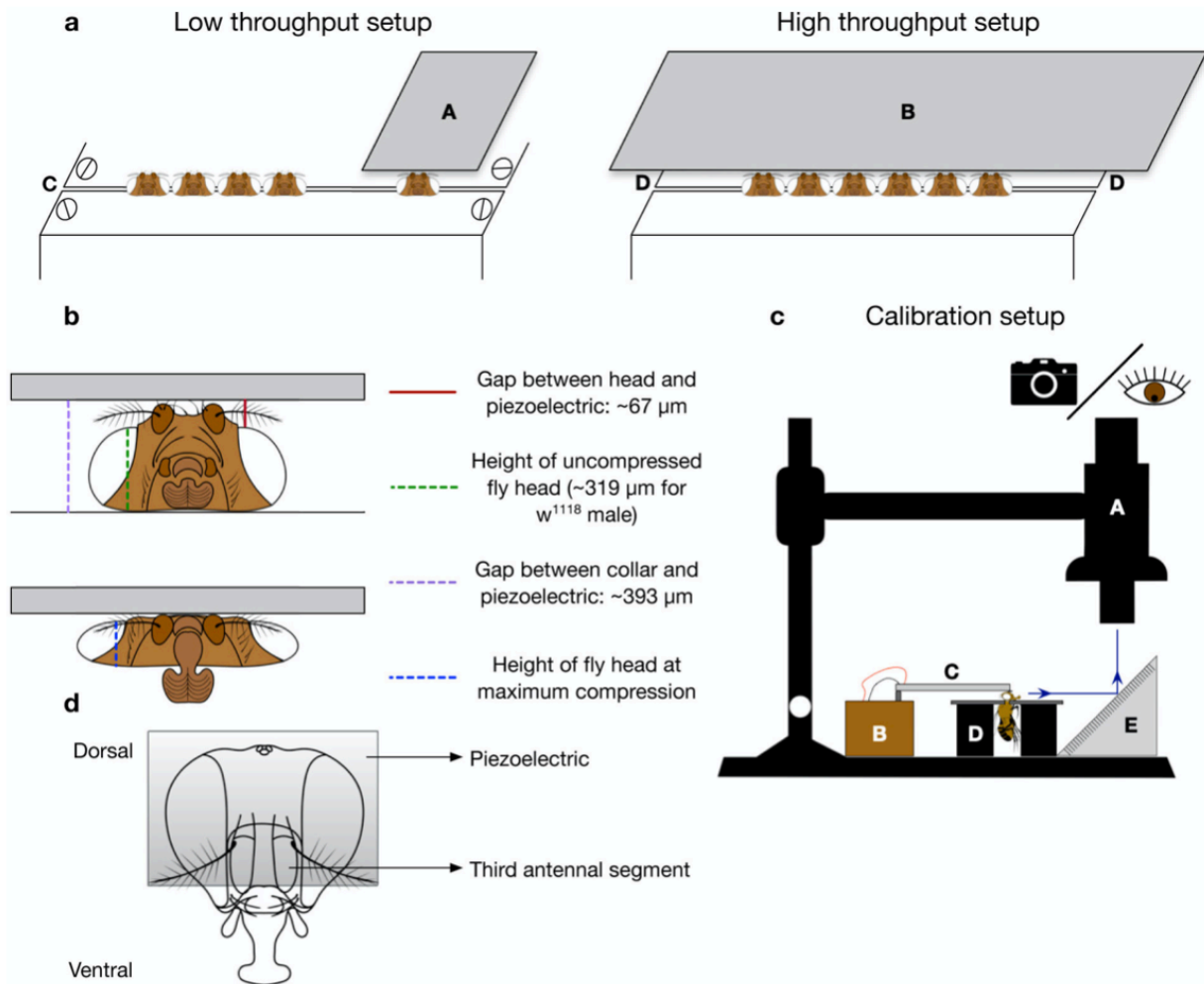
Figure 1-2 dTBI Device Setup and Calibration (Bonini Lab)[1]

CHAPTER 2

HYDROGEN GAS AND PINK1 MEDIATED RESCUE OF MITOCHONDRIAL
MORPHOLOGY IN MUSCLE TISSUE

2.1 Abstract

We investigate the therapeutic potential of hydrogen gas supplementation in mitigating

mitochondrial dysfunction and neuroinflammation in amyotrophic lateral sclerosis (ALS)

models. Hydrogen holds promise as an antioxidant in neutralizing ROS and RNS without

disrupting essential cellular signaling pathways. Using *Drosophila melanogaster* as a model

organism, we describe a novel method for hydrogen gas supplementation to flies via inhalation.

We investigate the effects of hydrogen treatment on ALS-associated genetic variants known to

disrupt mitochondrial morphology and protein expression, including TDP-43, FUS, and GR80.

Preliminary findings suggest that hydrogen gas supplementation attenuates mitochondrial

dysfunction and neuroinflammation in ALS models, offering potential therapeutic benefits.

Further elucidation of the molecular mechanisms underlying hydrogen's effects may provide

valuable insights into ALS pathogenesis and therapeutic interventions.

2.2 Background

Mitochondria play an essential role in cell survival and functioning, and their dysfunction

is profoundly linked to the pathogenesis of neurological disease.[12] As the site of oxidative

phosphorylation, mitochondria harness energy in the form of ATP, but they are also an essential

mediator in Ca2+ homeostasis, the synthesis of NAD+/NADH metabolites, and apoptosis.[13]

Neurons, in particular, require a high energy demand and rely on calcium ions for neuronal signaling, synaptic transmission, and excitability .[14]

One of the major negative effects of mitochondrial dysfunction and misfolded proteins is the overproduction of reactive oxygen and reactive nitrogen species (ROS and RNS).[15] ROS and RNS can damage macromolecules and organelles and create deficits in the energy supply, which can be particularly detrimental to proteostasis. ROS and RNS can also over-activate stress response pathways, ultimately leading to cell death.

Supplementation with hydrogen gas may be able to alleviate the negative effects of both ROS and RNS, including their overactivation of stress response pathways. Hydrogen functions as an antioxidant by directly reducing hydroxide radicals, inhibiting MAPK and excess calcium. If ROS is excessively mitigated, essential stress response pathways may be blocked, which would be detrimental to the cell. Hydrogen may be superior to other conventional antioxidants because it can reduce hydroxide radicals while preserving essential ROS that are otherwise used for normal cellular signaling.

To investigate the effects of hydrogen treatment on ROS, we tested 3 different genetic mutational variants for ALS: TDP-43, FUS, and GR80, each known for their detrimental effects on mitochondrial morphology and aberrant protein expression.

Tar DNA binding protein-43 (TDP-43) functions normally as an RNA-binding protein ubiquitously expressed in the nucleus of cells and contributes to synaptic growth of motor neurons and glial wrapping.[16] Cytoplasmic TDP-43 protein aggregates have been extensively studied for their role in cellular toxicity and degeneration in both inherited and spontaneous forms of Amyotrophic Lateral Sclerosis and frontotemporal lobar disease (FTLD).[17] Although aberrant TDP-43 has been linked to impaired RNA splicing, mitochondrial dysfunction, and a

disruption of protein homeostasis, the mechanism of aberrant TDP-43 formation and pathogenesis remains unknown.[18–20]

Fused in Sarcoma (FUS) is similar to TDP43. It is an RNA-binding protein that plays important roles in stabilizing pre-mRNA, RNA splicing, transport, and translation regulation.[21–23] It is predominantly localized in the nucleus but can shuttle between the nucleus and the cytoplasm. The line we will use is a transgenic line with the insertion of the FUS human gene.

GR80 artificially expresses 80 glycine-arginine (GR), repeats to model the G_4C_2 hexanucleotide repeat expansion in C9ORF72, the most frequent genetic cause of ALS.[24,25] GR80 has also been implicated in translational stalling and C-terminal extensions on the mitochondrial surface.[26]

Another pathological hallmark of ALS is the hyperactivation of neuroinflammatory pathways, such as NF-κB p65 and cGAS/STING pathways.[27,28] Excess translocation of TDP-43 into the mitochondria may promote this hyperactivation. In our experiments, we also investigate the blockage of TDP-43 translocation into the mitochondria by knocking down and out the PINK1 protein homolog and examining changes in mitochondrial area and morphology.

2.2 Methods

Drosophila stocks and fly culture

Flies were normally raised at 25°C, with a 12/12-hour dark/light cycle, with approximately 65% humidity on standard food receipt (17 L water, 93 g agar, 1,716 g cornmeal, 310 g brewer's yeast extract, 517 g sucrose, 1033 g dextrose), unless otherwise stated. Fly crosses were conducted according to standard procedures. Adult flies were collected after eclosion and divided into

separate vials (~20 flies per vial) for maturation, aging, and waiting for experiments. Vials were flipped every other day.

Hydrogen Treatment

To generate hydrogen gas, 50mL of 0.25 sodium hydroxide is reacted with 2 g of aluminum foil in an empty polyethylene container and placed inside a reaction chamber (supplementary table 2). This reaction takes place in the bottom of the chamber so that the hydrogen molecules may diffuse upward, filling the chamber. In the control container, we substituted sodium hydroxide with water to replicate the humid effects of the hydrogen molecules in the chamber. Flies are housed in plastic or glass vials with cotton tops so the hydrogen may diffuse into the vial, and the flies may inhale the gas (supplementary figure 1)

Mitochondrial morphology and immunohistochemical analysis

To reveal the mitochondrial morphology, mitoGFP protein was expressed in *Drosophila* indirect flight muscle (by *MHC-Gal4*). TDP-43 (WT and mutant A315) is endogenously fused to a red fluorescent protein reporter (RFP). For analysis of mitochondrial morphology in adult flies (brain and indirect flight muscle), male flies were first aged at 25°C for 5 days before tissue collection. In muscle staining, at least 5 independent replicates were dissected for each genotype.

For immunohistochemical examination of mitochondrial morphology, isolated fly thoraces and heads were fixed in PBSTx (1x PBS, 0.25% Triton X-100) with 4% formaldehyde. They were briefly washed, subsequently dissected and further blocked with 5% normal goat serum in 1x PBSTx for 60 minutes at room temperature. Samples were incubated with primary antibodies diluted in blocking buffer overnight at 4°C. The primary antibodies used here were rabbit anti-*Drosophila* Ref2p (1:500) and chicken anti-GFP (1:1000). After three 10 minutes of

washing steps with 1x PBSTx at room temperature, samples were incubated with fluorophore-conjugated secondary antibodies (1:500) for 3 hours at room temperature in the dark. After an additional three 10 minutes washing steps with 1x PBSTx at room temperature, samples were mounted on slides. The slides were subsequently investigated under a confocal fluorescence microscope (Zeiss). All confocal images were taken with a Zeiss LSM710 Meta confocal microscope and examined by the ZEN Blue Edition Software.

2.3 Results

2.3.1 Hydrogen Treatment Regulates Lifespan and Mitochondrial Dynamics of TDP-43 mutant models

For precise expression of TDP-43 genes in *Drosophila* muscle cells in lifespan experiments, we selected MHC>Gal-4 as a driver. Muscle fibers were chosen for their high number and concentration of mitochondria. We initially tested the lifespan of TDP-43.A315T mutant flies by dividing the flies into males and females and treatment and non-treatment (control) groups to control for both sex and hydrogen treatment. In our first trial, we see the hydrogen-treated group dramatically increased the lifespan of female flies compared to controls in the non-treatment group. Around 65% of treated flies remained compared to close to just 5% in the control group by day 23. There was no significant difference in lifespan in the male cohorts. Interestingly, the female TDP-43 flies from the non-treatment group died significantly faster than the males in this first lifespan trial (1A).

In addition to lifespan, mitochondrial morphology is an effective readout for cellular dysfunction. Chronically fragmented mitochondria produce more reactive oxygen species (ROS), more rapidly accumulate mutated mtDNA, become respiratory chain deficient, and are sensitized to apoptotic signaling. In contrast, fused mitochondria emit less ROS, accumulate fewer mutated

mtDNA, are less susceptible to proapoptotic signaling, and may exhibit greater energetic efficiency.[29] Mitochondria may fuse together as a short-term response mechanism to metabolic undersupply and cellular stress, including ROS/RNS; however, during times of chronic stress, mitochondria may fragment. Thus, mitochondria morphology provides key insights into both the health of the cell and ROS/RNS levels.[30]

To test whether hydrogen supplantation may directly mitigate the morphological effects associated with ROS/RNS, we crossed TDP-43.A315 with MHC>mitoGFP to express GFP endogenously in the mitochondria of muscle cells. Mitochondria morphology was examined at days 0, 5,10, and 15 in both sexes and treatment/non-treatment groups (1B) and quantified by mean mitochondrial form and mean area (1C,D).

Mitochondrial form factor is defined as a measure of its overall shape complexity and is calculated by dividing the perimeter of mitochondria by the square root of the area.[31]

Equation 1:

$$Form\ Factor = \frac{Perimeter}{\sqrt{area}} = \frac{P^2}{(4\pi A)}$$

Quantifying the form factor represents how convoluted or branched the mitochondrion's perimeter is relative to its size. A higher form factor value indicates more elongated and irregularly shaped mitochondria with complex branching or convolutions, while a lower value of 1 indicates more compact or fragmented mitochondria.[31] In our quantification of the mitochondrial form factor in the TDP-43 mutant model, we do not see a statistically significant difference between any control and treatment groups within the same sex and time points. In other words, there was no difference between the control and treatment mitochondrial form factors in the TDP43 male cohorts at days 5 and 10 or the female cohorts at days 10 and 15. However, we did see significant differences in morphologies across time points.

When comparing males at day 0 with control and treatment groups at day 5, no statistical differences in form factor were observed. Additionally, no statistical differences were found between males in both treatment and non-treatment groups at days 5 and 10. This includes comparisons between day 5 control and day 10 control, day 5 treatment and day 10 treatment, or day 5 control and day 10 treatment.

Over a longer time, horizon, comparing males at day 0 with non-treatment males at day 10 revealed a significant decrease (*$p < 0.05$) in form factor in the control groups, indicating mitochondrial fragmentation over a 10-day period. In contrast, no statistically significant difference in mitochondrial form factors was found between day 0 and day 10 males undergoing hydrogen treatment.

On days 10 and 15, the mean form factors of female non-treatment groups remained unchanged; however, the mean form factor of the treatment groups dramatically decreased from day 10 to day 15, indicating increased fragmentation. Although increased fragmentation may be indicative of chronic stress, there was no significant difference in the form factor or mean areas on treatment day 15 compared to the baseline mean form factor or mean areas on day 0. This suggests that mitochondria may be returning to normal conditions, aligning with our lifespan data showing TDP-43 treatment groups living significantly longer than non-treatment groups.

Additional differences in mitochondrial form factor were observed when comparing different sexes at the same time points. For example, at day 10, female controls had a significantly larger (*$p < 0.05$) form factor than male controls. Similarly, the female treatment groups exhibited significantly larger mitochondria form factor (**$p < 0.01$) than the male cohorts at day 10.

Figure 1
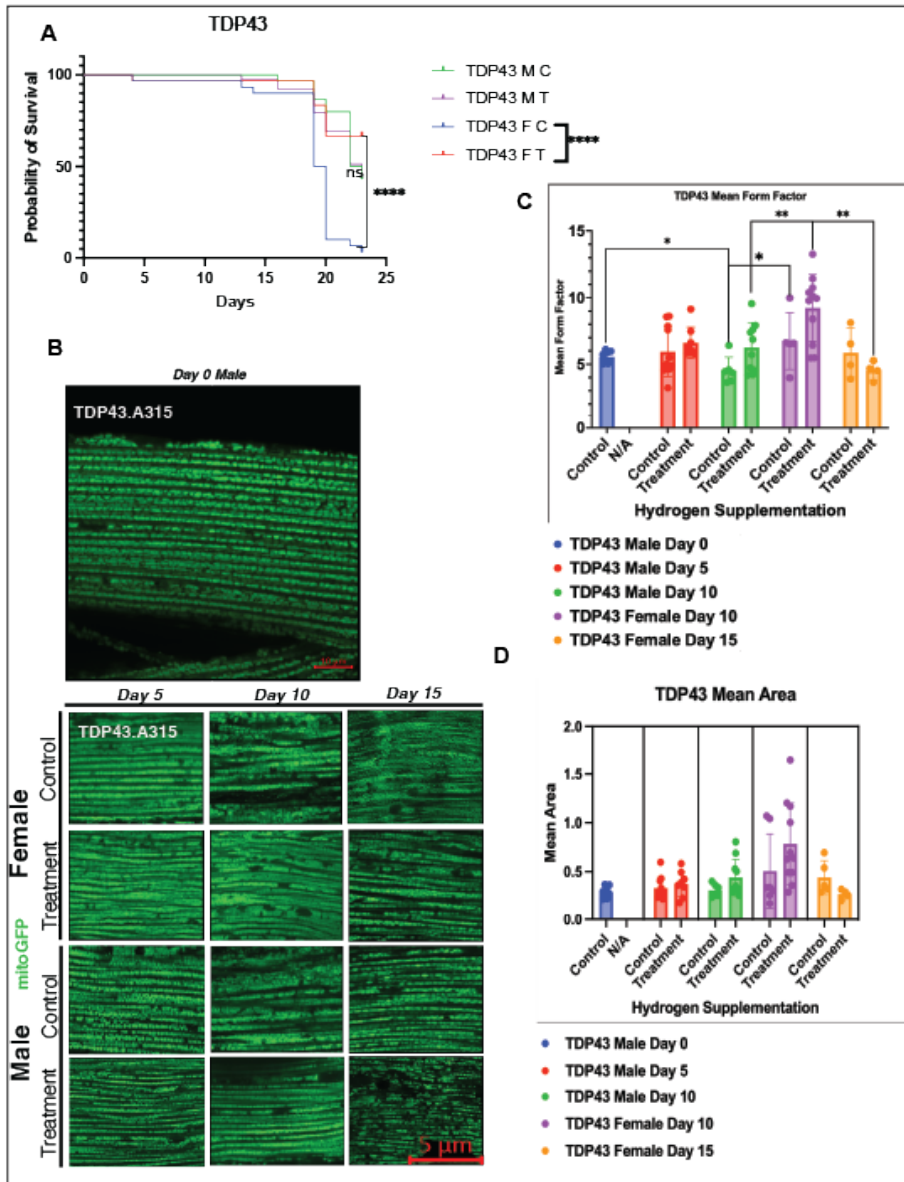
Figure 2-1 Hydrogen Treatment Regulates Lifespan and Mitochondrial Dynamics of TDP-43 mutant models.
A) Kaplan-Meyer lifespan curve. 30 TDP-43.A315 flies per vial per genotype. Hydrogen Treatment twice per day. Significance was calculated using the Mantel-Cox test. Legend: M = males; F = females, C = control (non-treatment) group, T = Treatment group). Female Treatment lifespan (red) was significantly longer than the TDP-43 female non-treatment group (blue) B) Immunostaining shows mitochondrial morphology of TDP-43.A315 mutants in wild-type fly muscle. Day 0 (left) male flies. Day 5 shows non-treatment control (top) vs treatment (bottom). Day 10 shows male non-treatment control (top) vs treatment (bottom). Day 15 shows non-treatment (top) vs treatment (bottom). Mitochondrial morphology is monitored using the mitoGFP reporter Scale bars, 5 μm. C) Quantification of mitochondrial mean form factor from . D) Quantification of mitochondria mean area. Significance was calculated using 2-sample t-test. number of images (n) = {(control: day 0 M:8, day 5 M:12; day 10 M: 6, day 10 F: 5; day 15 F:4) (Treatment: day 5 M:8; day 10 M: 10, day 10 F: 11; day 15 F:4)} *(p<0.05), **(p<0.01),***(p<0.001), **** (p<0.0001).

2.3.2 Hydrogen Treatment Regulates Lifespan and Mitochondrial Dynamics of FUS mutant models

FUS mutations were again expressed in *Drosophila* muscle cells using MHC>Gal-4 driver in lifespan experiments. Unlike TDP-43 in our first TDP-43 trial, we do not see a significant difference in any of the FUS cohorts (2A).

In our investigation of FUS mutant mitochondria morphology, we expressed FUS.525L using MHC>mitoGFP driver (2B). As in TDP-43, we observed distinct patterns in mitochondrial morphology across different time points and sexes. On Day 10, there was a significant decrease in mitochondrial form factor in females compared to non-treatment controls ($*p<0.05$). No significant differences were observed in males at Day 10 or in any control and treatment groups at Day 0 and Day 10. Notably, at Day 0 and Day 5, control females exhibited a significant decrease in form factor ($**p<0.01$), which was not observed in treatment females. Treatment females at Day 10 showed a significant decrease in form factor compared to Day 0 ($**p<0.001$), indicating increased mitochondrial fragmentation. Across time points, no significant differences were observed in form factor between Day 5 and Day 10 control females; however, treatment females exhibited a significant decrease in form factor ($**p<0.01$). Unlike TDP-43, FUS females undergoing treatment at day 10 had a lower mean form factor and mean area than baseline at day 0. Comparison between males and females revealed that on Day 10, female controls had a significantly larger form factor than male controls ($*p<0.05$). Similarly, treatment females exhibited larger mitochondria form factor than males ($**p<0.01$). Overall, our FUS mutant data

indicate differential effects on mitochondrial morphology, with treatment females showing

increased fragmentation compared to controls, particularly at later time points. (2C, 2D).

Figure 2

2.3.3 Hydrogen Treatment Regulates Lifespan and Mitochondrial Dynamics of GR80 mutant models

Examining the lifespan of GR80 mutant cohorts, we observe a significant decrease in the lifespan of males undergoing treatment compared to their control and no significant difference in the lifespan of the females. (3A)

In our analysis of GR80 morphological data, we observed distinct patterns in mitochondrial form factors across different time points and sexes. (3C, 3D) On Day 5 and Day 10, both males showed no significant differences in form factor compared to non-treatment controls, indicating similar mitochondrial morphology between treatment and control groups. On day 5, females exhibited no differences between control and treatment groups, but on day 10, female treatment flies exhibited slightly more fragmented morphology (*p<0.05). Comparison between treatment and control groups at different time points revealed no statistically significant differences in form factor for males, except for a significant increase in morphology between Day 5 control and Day 10 treatment males (**p<0.01), indicative of mitochondrial fusion.

For females, there were no significant differences in form factor between treatment and control groups at Day 0 and Day 5. However, comparing baseline at day 0 to day 10, treatment females exhibited a very significant decrease in form factor (****p<0.0001), while control females also showed a significant but less dramatic decrease (**p<0.01). Furthermore, significant fragmentation was also observed between Day 5 and Day 10 control females

(**p<0.01) and between Day 5 and Day 10 treatment females (****p<0.0001), as well as between Day 5 control and Day 10 treatment females (*p<0.05).

When comparing males and females at Day 0, Day 5, and Day 10, no significant differences in form factor were observed on days 0 and 5; however, at Day 10, both control and treatment males exhibited a significant increase in form factor compared to females (***p<0.001 and **p<0.01, respectively).

Overall, our GR80 mutant data suggest drastic sex differences in mitochondrial morphology in reaction to hydrogen treatment. Increased mitochondrial fusion was observed over a 10-day period in males, while the opposite effect, increases in fission, was observed over a 10-day period in females. Even without hydrogen treatment, female flies exhibit increased mitochondrial fragmentation over time, but hydrogen appears to exacerbate these effects.

2.3.4 Lifespan Kaplan Meyer Curve Repeat of flies undergoing hydrogen treatment

We repeated the lifespan trial using TDP-43 and FUS mutants under the MHC>gal-4 driver using 50 flies per cohort. In the FUS group, we see the effects of hydrogen gas detrimentally affecting the female and male cohorts with around 95% survival for the control group vs. about 45% for the treatment group This aligns with our morphological data comparing day 10 treatment females with day 0 flies, the day 10 flies having more fragmented mitochondria than baseline and non-treatment group at day 10.

Figure 3

A GR80

Probability of Survival vs Days

GR80 M C
GR80 M T
GR80 F C
GR80 F T

ns

B

Day 0 Male

GR80

5 μm

Day 5   *Day 10*

GR80

Female Control / Treatment

Male Control / Treatment

mitoGFP

10 μm

5 μm

C GR80 Mean Form Factor

Mean Form Factor

Hydrogen Supplementation

Control N/A Control Treatment Control Treatment Control N/A Control Treatment Control Treatment

● GR80 Male Day 0
● GR80 Male Day 5
● GR80 Male Day 10
● GR80 Female Day 0
● GR80 Female Day 5
● GR80 Female Day 10

D GR80 Mean Area

Mean Area

Hydrogen Supplementation

Control N/A Control Treatment Control Treatment Control N/A Control Treatment Control Treatment

● GR80 Male Day 0
● GR80 Male Day 5
● GR80 Male Day 10
● GR80 Female Day 0
● GR80 Female Day 5
● GR80 Female Day 10

Figure 3 Hydrogen Treatment Regulates Lifespan and Mitochondrial Dynamics of GR80 mutant model.. A) Kaplan-Meyer lifespan curve. 30 FUS.P525L flies per vial per genotype. Hydrogen Treatment twice per day. Significance was calculated using the Mantel Cox test. Legend: M = males; F = females, C = control (non-treatment) group, T = Treatment group).Significant differences * (p<0.05) between males of GR80 treatment (purple) and male non-treatment groups (green); Non-significant (ns) difference between females of GR80 treatment (red) and female non-treatment groups (blue). B) Immunostaining shows mitochondrial morphology of GR80 mutants in wild-type fly muscle. Day 0 (left) male flies. Day 5 shows non-treatment control (top) vs treatment (bottom). Day 10 shows male non-treatment control (top) vs treatment (bottom) Mitochondrial morphology is monitored using the mitoGFP reporter Scale bars, 5 μm. C) Quantification of mitochondrial mean form factor. D) Quantification of mitochondria mean area. Significance was calculated using 2-sample t-test. *(p<0.05), **(p<0.01),***(p<0.001), **** (p<0.0001{(control: day 0 M:2, day 5 M:4; day 10 M: 2, day 0 F: 7; day 5 F:3; day 10 F: 8) (Treatment: day 5 M:7; day 10 M: 5; day 5 F: 5, day 10 F: 3)} *(p<0.05), **(p<0.01),***(p<0.001), **** (p<0.0001

In the TDP-43 cohort we again observe a dramatic rescue of TDP43 female flies when treated with hydrogen compared to the males. At around day 25 around 10% of the control group TDP43 females were alive, while around 60% of the treatment group TDP43 females remained. Again, there was no significant difference between the maleTDP-43 control and treatment groups.

Notably, in the homozygous MHC>gal 4 control group flies, both treatment and nontreatment groups saw a higher mortality than FUS control. In the Male cohort, the control group MHC>Gal4 had higher survival rates, closer to what we might expect, and higher than the disease models. Again, there was no significant difference between the TDP-43 control and treatment groups.
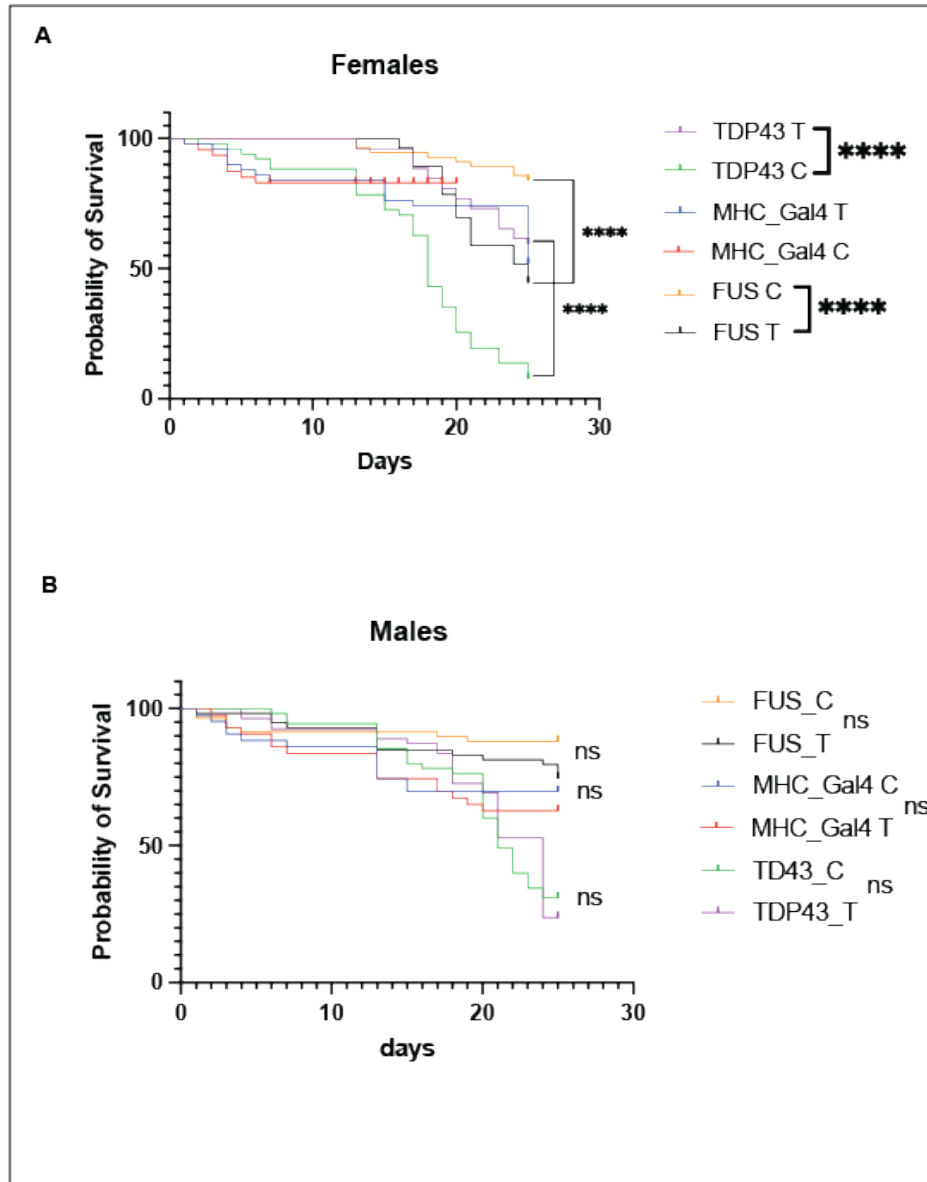
*Figure 4 Lifespan Kaplan Meyer Curve Repeat of flies undergoing hydrogen treatment. 50 flies per vial per genotype. Hydrogen Treatment twice per day. Significance was calculated using the Mantel-Cox test. A) Females. TDP-43 female Treatment lifespan (black) was significantly longer **** (p<0.0001) than the TDP-43 female non-treatment group (yellow). FUS.P52L female treatment group lifespan (purple) is significantly shorter **** (p<0.0001) than FUS.P52L female non-treatment (green). Non-significant (ns, p<0.05) differences between females of MHC>Gal-4 treatment (blue) and females in non-treatment groups (red). B) Males. Non-significant (ns, p<0.05) differences between males of TDP-43 treatment (purple) and non-treatment groups (green); Non-significant (ns, p<0.05) differences between males of FUS.P52L treatment (black) and non-treatment groups (yellow). Non-significant (ns, p<0.05) differences between males of MHC>Gal-4 treatment (red) and male non-treatment groups (blue).*

Figure 5
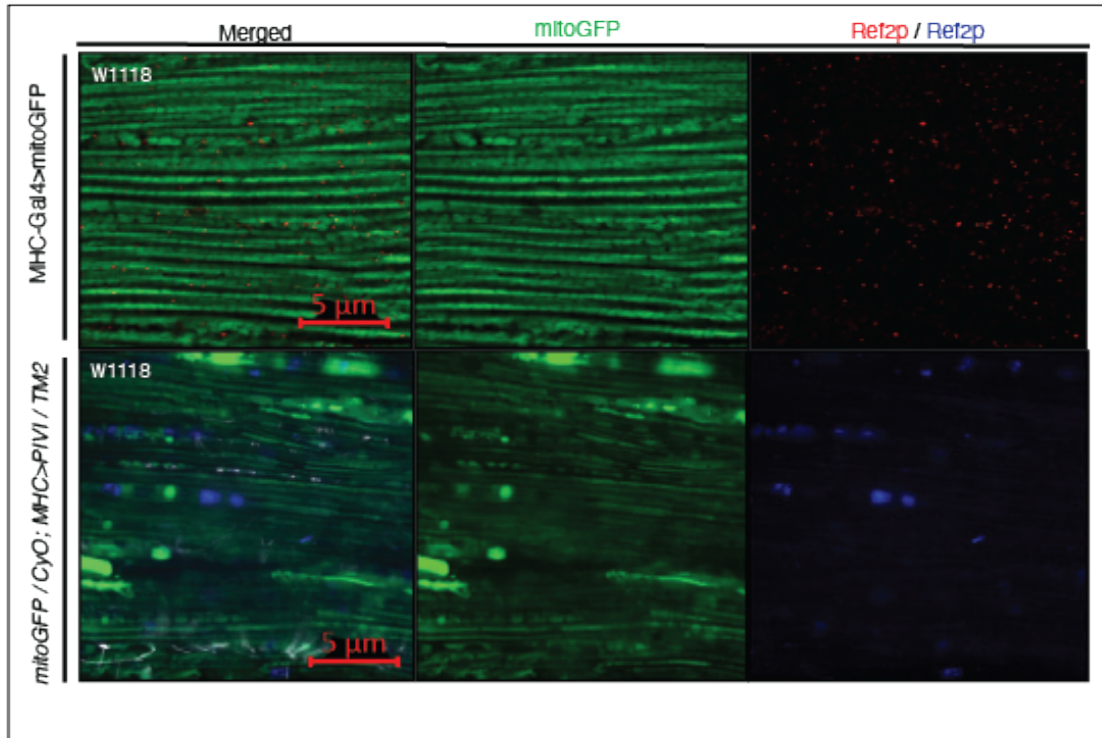
Figure 5 Pink1 KD (pivi) regulates mitochondria morphology in W1118 flies. (Top) Immunostaining showing normal mitochondrial morphology in control: w1118 crossed with MHC>mitoGFP; mitochondrial morphology is monitored using mitoGFP reporter (green), and autophagy is monitored using ref2p marker (red). (Bottom) Immunostaining showing normal, abnormal mitochondrial morphology and increased autophagy in pink1KD flies: w1118 crossed with mitoGFP/CyO; MHC>pivi/TM2; mitochondrial morphology is monitored using mitoGFP reporter (green), and autophagy is monitored using ref2p marker (blue). Flies were ages for 5 days. Scale bars, 10 μm.

We next sought to investigate TDP-43's interaction with the mitochondria. Recessive mutations in PINK1 and Parkin genes are known as inherited forms of Parkinson's disease. PINK1 is a mitochondrial kinase active in mitochondrial quality control, protein translocation into the mitochondria, and regulation of mitochondrial fission/fusion dynamics.[32] PINK1 exists in a common pathway with parkin and is stabilized and under stress conditions on the outer membrane of the mitochondria, where it activates parkin, an E3 ubiquitin ligase that begins the mitophagy process.[33]

We used P62 analog Ref2P as an autophagy marker for ubiquitinated protein aggregates stained in blue.

Figure 5 establishes the control group. W1118 is crossed with MHC>mitoGFP and MHC>mitoGFP PIVI, the drosophila homolog of PINK1 knockdown. The mitochondrial aggregation and increased Ref2P signal immediately show the importance of Pink1.

In Figure 6A, we crossed both WT and mutant TDP43 to the pivot driver; we saw a striking rescue of this phenotype. In both WT and mutant TDP43 models, mitochondria appear normal, and the TDP-43 protein in red resides in the nucleus. UAS-RFP serves as a control; red fluorescent protein is expressed in muscle cells in the control and TDP43 protein in WT and mutant variants. DAPI is also used as a marker of the nuclei.

Comparing WT and mutant forms of TDP-43 to FUS expressed in muscle FUS muscle cells and crossed with Pink1, we see severe mitochondrial aggregation and increased ref2P signal, especially in the FUS mutant. (6B)

To confirm this knockdown and rescue, TDP 43 was crossed to PINK1 knockout driver B9 MHC>mitoGFP (7A,B) . A similar phenotype and rescue in mitochondrial morphology is observed. Notably, the TDP-43 signal appears slightly more dispersed in the cytoplasm compared to the knockdown variant and mutant model.

We then aged these flies 15 days (6B). In WT TDP43, TDP43 RFP signal has clearly diffused out of the nucleus and into the cytoplasm and fragmented mitochondria. In the mutant model, we see severe mitochondrial aggregation and dispersion of TDP-43 out of the nucleus. Ref2P could be slightly increased in TDP-43 mutant, mutant quantification via fluorescent intensity or western is needed for confirmation.

Figure 6
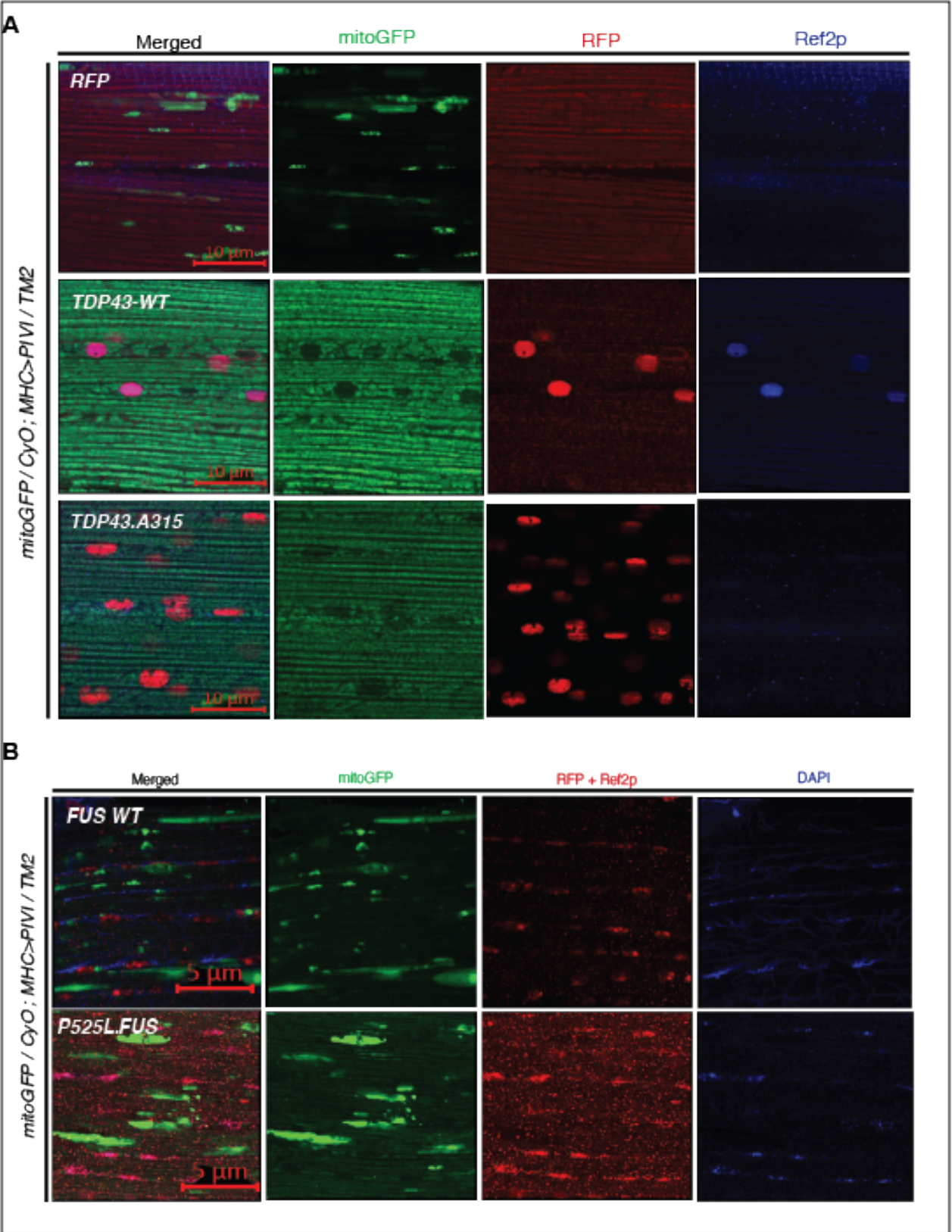
Figure 6 TDP-43.A315 and TDP43-WT rescue abnormal morphology in Pink1 knockdown (KD) flies. A) Immunohistological staining of RFP (control), TDP-43.WT, and TDP-43.A315T, crossed with Pink1 KD (pivi). Mitochondrial morphology and autophagy are rescued in both TDP-43 mutant and WT, and TDP-43 is localized normally to the nucleus. Mitochondrial morphology is monitored using mitoGFP reporter (green), endogenous TDP43 is measured using red fluorescent protein reporter (red), and autophagy is monitored using ref2p marker (blue). Flies were aged for 5 days. Scale bars, 10 μm. B) Immunostaining showing abnormal mitochondrial morphology, ubiquitous expression of FUS, and increased autophagy in FUS.P52L mutant and FUS.WT flies co-expressing pink1KD; mitochondrial morphology is monitored using mitoGFP reporter (green), autophagy and endogenous FUS are both monitored using ref2p marker and red fluorescent protein reporter (red), and nuclear morphology is stained by DAPI (Blue). Flies were aged for 5 days. Scale bars, 10 μm.
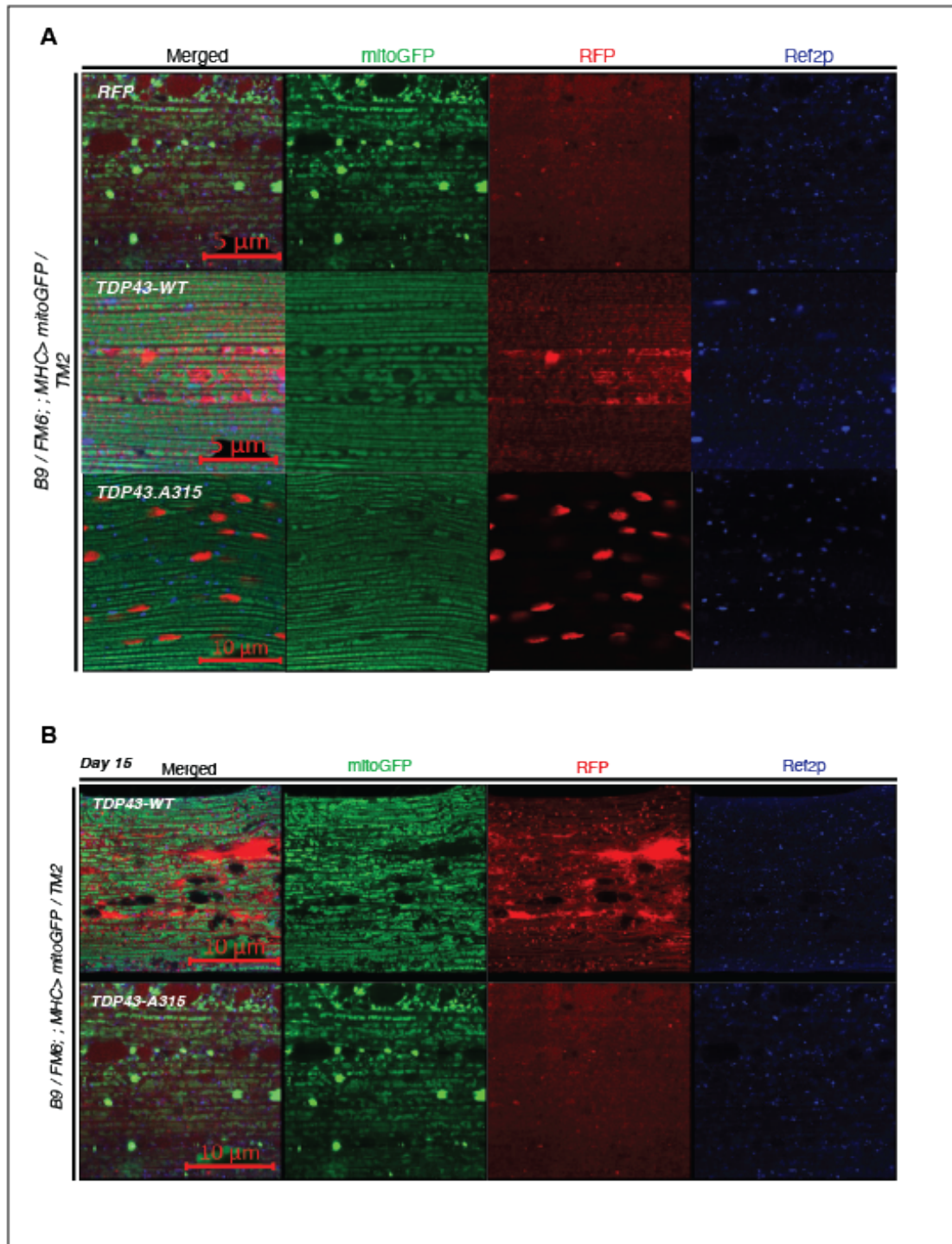
Figure 7

Figure 7 TDP-43.A315 and TDP43-WT rescue abnormal morphology in 5-day-old Pink1 knockout (KO) flies but not 15-day-old. A) Immunohistological staining of RFP (control), TDP-43.WT, and TDP-43.A315T, crossed with Pink1 KO (B9). On day 5, mitochondrial morphology and autophagy are rescued in both TDP-43 mutants and WT, and TDP-43 is localized normally to the nucleus. Mitochondrial morphology is monitored using a mitoGFP reporter (green), endogenous TDP43 is measured using a red fluorescent protein reporter (red), and autophagy is monitored using a ref2p marker (blue). Scale bars, 10 μm. B) When aged to 15 days, mitochondrial morphology appears abnormal and TDP-43 has localized to the cytoplasm in both WT and mutant TDP-43. Autophagy appears to have decreased, but confirmation is needed. Mitochondrial morphology is monitored using a mitoGFP reporter (green), endogenous TDP-43 is monitored using a red fluorescent protein reporter (red), and autophagy is monitored using a ref2p marker (blue). Scale bars, 10 μm.

Discussion

Through both lifespan trials, hydrogen significantly increased the survival of female flies expressing TDP-43, while no significant effect of hydrogen supplementation was observed in male flies expressing TDP43. In the first trial, we saw a detrimental effect of hydrogen supplementation compared to the non-treatment group in the GR80 male cohort and a non-significant difference between both the male and female cohorts. In contrast, in the second trial, we saw a significant decrease in the lifespan of females undergoing hydrogen treatment compared to the non-treatment group.

Our morphological data of mean form factors aligns with the lifespan data in some aspects but not others. For example, we observe an increased fermentation in the day 10 female FUS flies undergoing treatment below baseline at day 0, which is indicative of chronic stress and cellular dysfunction leading to death, but we do see this effect in the morphology in the FUS female flies not undergoing treatment.

Key limitations across both lifespan trials include the lack of a proper control group. In the first trial, I did not include homozygous MHC>Gal 4, and in the second trial, my MHC>Gal 4 flies died unexpectedly soon in the male cohort. This may be due to weak genetic background of this cohort of flies and warrants repeating. A weak genetic background may be indicative of problems in the genetic background of our disease model data of trial 2, but this seems unlikely

considering the significant decrease ($p<0.0001$) in the lifespan of the MHC>Gal 4 non-treatment group compared to FUS non-treatment males. Another key limitation is a lack of morphological data longer than day 10 and day 15, as the flies begin to die more rapidly across disease models past day 20.

Future experiments include confocal imaging of hydrogen treatment at time points past day 20, a third lifespan trial including GR80 mutants and proper control, and the inclusion of wildtype TDP-43 and FUS lines.

Further investigating the role of TDP-43 in mitochondrial morphology and dynamics, we found that Pink1 knockdown and knockout dramatically rescue mitochondrial morphology in 5-day-old flies. This effect is not seen at 15 days. Another future experiment may include hydrogen treatment of TDP-43 flies, both WT and mutants, expressing Pink1 knockdown or knockout and investigating their lifespan and morphologies for alleviation. Hydrogen may alleviate some of the effects we see in figure 7B at day 15.

CHAPTER 3

40S RIBOSOMAL SUBUNIT RECYCLING FACTORS USP10/USP10 AND RIN/G3BP1
REGULATE MITOCHONDRIAL MORPHOLOGY

3.1 Abstract

Proteostasis, the finely tuned orchestration of protein synthesis, folding, trafficking, and degradation, is vital for cellular homeostasis and viability. Central to proteostasis is the regulation of protein translation, a process fraught with potential errors that can lead to the accumulation of misfolded proteins and cellular dysfunction. Our research focuses on elucidating the intricacies of protein translation quality control mechanisms, particularly within the context of ribosomal quality control (RQC). RQC is a multi-step process activated in response to ribosomal stalling, ensuring the fidelity of protein synthesis and preventing the release of aberrant proteins into the cellular milieu. We explore the implications of inefficient RQC on cellular function, particularly in the context of lifespan. Dysregulation of RQC can lead to the formation of aberrant protein aggregates, posing a significant threat to mitochondrial integrity and function. Specifically, we identify the involvement of the USP10-G3BP1 complex in mediating the recycling of ribosomal 40S subunits and reveal its connection to cellular energy metabolism.

3.2 Background

Protein homeostasis "proteostasis", refers to the balanced regulation of protein synthesis, folding, trafficking, and degradation within cells.[34] It is essential for maintaining cellular

function and preventing the accumulation of misfolded or aggregated proteins, which leads to cellular dysfunction and toxicity.[34]

All these pathways are interlinked in some way, but our laboratory primarily focuses on the aspect of protein translation in proteostasis, specifically the quality control mechanisms involved. The quality control mechanisms involved in co-translation mRNA decay by the exosome are the nonsense-mediated RNA decay pathway, no-go decay pathway, and non-stop pathway.[35] Examples of quality control mechanisms involved in nascent polypeptide and protein degradation by the proteosome are ribosome-associated quality control, heat shock response, and the ubiquitin-proteasome response.

RQC is a multi-step process in response to ribosomal stalling. Stalling can be caused for different reasons, including mRNA or tRNA with abnormal features or damage, immature ribosome produced by defective 60S subunit biogenesis, nonstop mRNA generated by endonuclease cleavage, or nonstop mRNA generated by premature mRNA polyadenylation.[36] These disruptions can be caused by gene mutations, errors during gene expression, chemical damage, or the absence of an interacting partner are examples of potential disrupters to these processes. [37]

The RQC model consists of four stages. In the first stage, the ribosomal subunits are rescued. Upon translation stalling, disomes or trisomes are first sensed by the ZNF598-RACK1 complex, which recognizes the 40S-40S interface of collided ribosomes.[38] ZNF598 then reversibly monoubiquitinates the ribosomal small subunit protein RPS10, and RNF10 (RING finger protein 10) monoubiquitinates RPS2 and RPS3.[38] The RACK1 complex then disassembles the collided ribosomes and allows the ABCE1-PELO-HBS1L to split it into the 60S (large) and

40S (small) subunits at the 3' end of the mRNA. The release mRNA is then degraded by the exosome. [39]

The second stage initiates the assembly of the RQC machinery on the 60S ribosomal subunit where the nascent chain is embedded. NEMF (nuclear export mediate factor, homolog in *Drosophila* is Clbn) binds to the 60S subunit, which then recruits and stabilizes E3 ubiquitin-protein ligase LTN1. [39]

The third stage involves extracting the stalled nascent polypeptide using the CAT-tailing mechanism. NEMF synthesizes carboxy-terminal alanine and threonine (CAT) tails to help expose lysine residues buried in the ribosomal exit tunnel to be ubiquitylated by Ltn1/listerin. VCP extracts nascent polypeptides from the 60S ribosomal subunit after they have been released from the conjugated tRNA by ANKZF1.[40] Finally, the fourth stage involves the degradation of the extracted nascent peptides by the proteasome.

In summary, the mechanism of targeting the state of translation rather than the folding state of the nascent polypeptide is evolutionarily advantageous to the cells because it can use machinery to recognize aberrant proteins before they are released for folding.

RQC machinery is typically sub-stoichiometric to ribosomes. As a result, inefficient quality control of the NPC-60S complex can happen, leading to the formation of aberrant NPCs containing C-terminal Ala and Thr additions (CAT-tails).[41] Failure to remove aberrant CAT tails can be particularly detrimental if CAT tails are aggregated during co-translation into organelles, such as the mitochondria or ER complex.[40] Previous studies revealed a correlation between CAT-tailing of mitochondrial complex I-30KD subunit and cellular toxicity based on genetic manipulation of the RQC pathway in the PINK1 model of Parkinson's disease. [42]

The 40s ribosome subunit Is much less studied compared to the CAT tail and the 60s recycling process. After NEMF binds to the 60s ribosome for the initiation of RQC, the 40S subunit is deubiquitinated and recycled by the G3BP1-family-USP10 complex.[43]

G3BP-1 or Ras GTPase-activating protein-binding protein 1 is an evolutionarily conserved protein in the RNA binding family that localizes in the cytoplasm and nucleus to regulate RNA metabolism.[44] Importantly, G3BP-1 proteins have been found to be a marker of stress granule formation.[45] Stress granules are membranelles organelles found in the cytoplasm of cells. They are formed in response to various stresses that inhibit translation, such as heat shock, oxidative stress, viral infection, or nutrient deprivation.[46] The inhibited mRNA and RNA binding proteins resulting from these stressors, such as stalled 48S pre-translational initiation complex and G3BP1.

Stress granules naturally harbor misfolded or premature proteins that may be cytotoxic or insoluble.[46] Under periods of prolonged stress, stress granules themselves can become insoluble aberrant and contribute to protein aggregation and the formation of pathological aggregates, such as those seen in Alzheimer's and amyotrophic lateral sclerosis (ALS).[44,47,48]

USP10 is a deubiquitinase involved in many different pathways, but its substrates are most often various stress modulators, like AMPK, which suggests that it has key functions in programmed cell death in response to the cell's energy status.[49] The USP10/G3BP1 complex is also found to control to de-ubiquitinate the 40S ribosomal subunit for recycling in RQC. Putting these two known functions in cellar energy metabolism and RQC together, our lab hypothesizes that the USP10-G3BP1 complex may connect RQC to energy metabolic pathways, but the exact mechanism has not been explored.

3.2 Methods

Drosophila stocks, fly culture, and drug treatment

The resources of Drosophila stocks used in this study were listed in the Key Resources Table. Flies were normally raised at 25°C, with a 12/12-hour dark/light cycle, with approximately 65% humidity on standard food receipt (17 L water, 93 g agar, 1,716 g cornmeal, 310 g brewer's yeast extract, 517 g sucrose, 1033 g dextrose), unless otherwise stated. Fly crosses were conducted according to standard procedures. Adult flies were collected after eclosion and divided into separate vials (~20 flies per vial) for maturation, aging, and waiting for experiments. Vials were flipped every other day.

For drug administration in _Drosophila_, Instant _Drosophila_ medium (1 g dry powder) was prepared from Millipore water (5 mL) mixed with DMSO (as the vehicle, 0.5%), Apigenin (10 mM), sulfaquinoxaline (100 µM). 10 young (within 5 days after eclosion) male flies were placed into each vial, and 4~5 biological replicates (4~5 independent vials) were examined per dose per genotype. Vials were flipped every day. Samples were collected for further analysis after 7 days of treatment.

3.3 Results

Figure 1

A

Actin Gal 4   Da Gal4

B
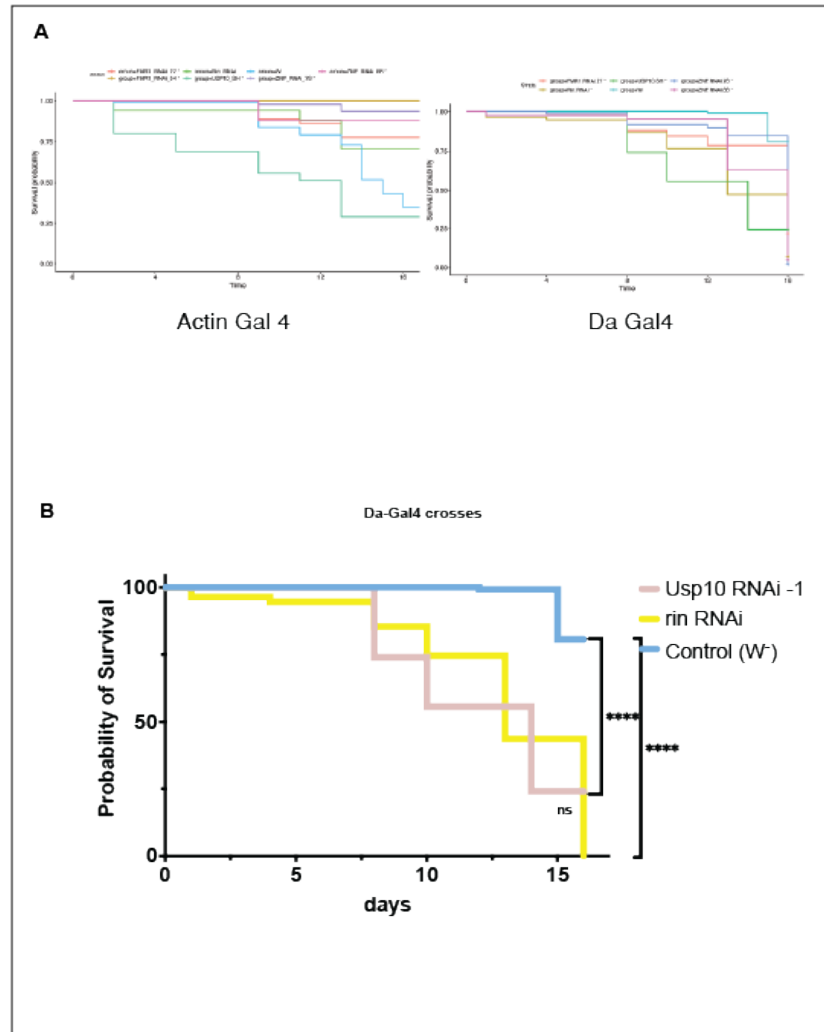
Figure 1 Screen for Gal 4 Drivers of RQC Gene Expression | A) Actin Gal4 and Da-Gal 4 whole body expression. 100 flies per group. 5 vials of 20 flies B) Da-Gal4 whole body expression repeat. Flies per vial Significance tests were significant under a Mantel-Cox test. 50 flies per group. 2 vials of 25 flies.

3.3.1 Genetic Screening for Drivers of RQC Genes

To better understand the role of USP10, rin, and other RQC genes in 40S ribosome recycling and mitochondrial dynamics, we first screened multiple different genetic drivers of our genes of interest in drosophila. I screened Da-Gal 4 and Actin Gal-4 for ubiquitous expression in neurons and in the cytoskeleton structure. Using Da-Gal4, we observed a significant decrease in lifespan between W- control and knockdown of Usp10 and rin, establishing their importance in

43

the fly's survival. (1B) I also screened for Pan-neuronal tissue (driven by 1407-Gal4). (1A) These drivers caused severe fitness decline of offspring, e.g., death or severe reduction in numbers and significant shortening of lifespan in flies that did survive. Ultimately, we found that MHC-Gal4 expressed in muscle is a suitable driver, as overexpression results in observable phenotypes, whereas knockdown is not lethal.

A
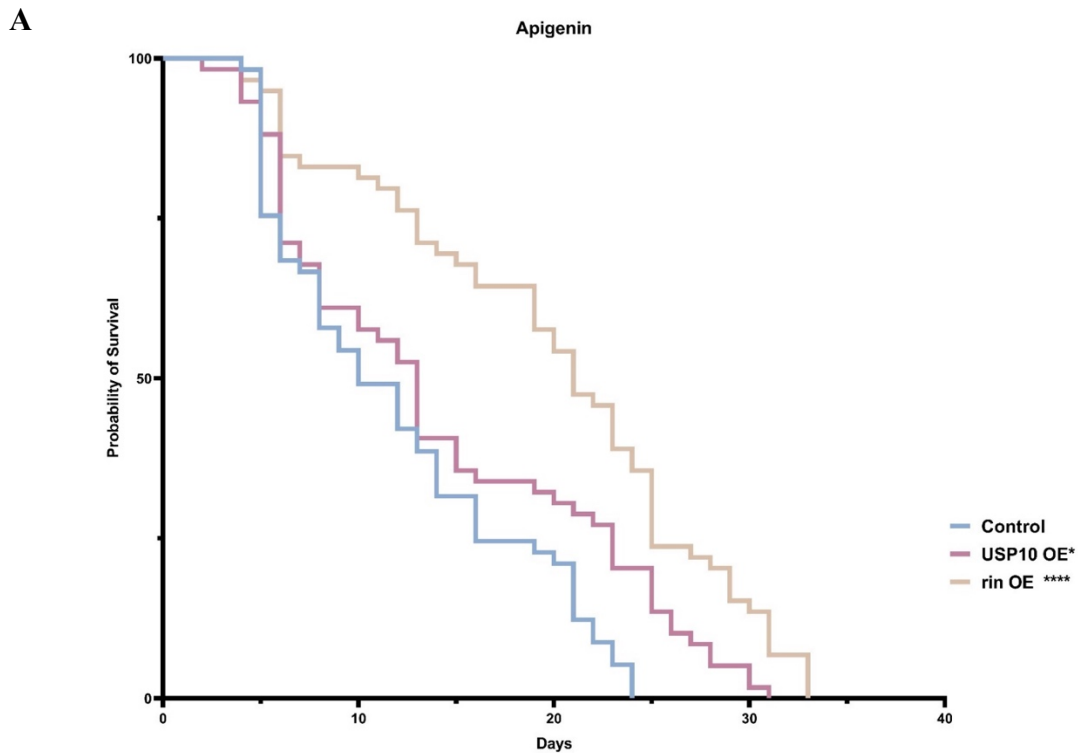
Apigenin

B
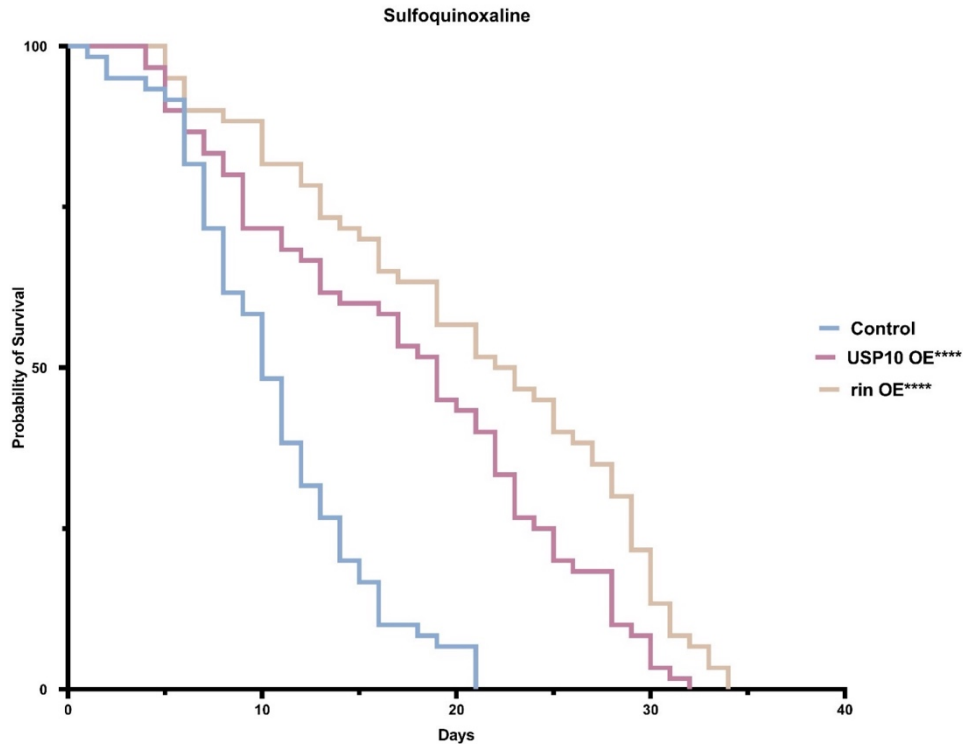
Figure 2 Apigenin and Sulfoquinoxaline induced read-through translation of USP10 OE and G3BP1 OE | A) 100 flies were placed at 25° for 3 days and then placed on fly food with 100 μ apigenin in DMSO. Flipped every 2 days. B)) 100 flies were placed at 25° for 3 days and then placed on fly food with 100 μ sulfoquinoxaline in DMSO. Flipped every 2 days. Significance tests were significant under a Mantel-Cox test.

3.3.2 USP10/Usp10 and G3BP1/rin rescue ribosome and protein toxicity

Overexpression of *Usp10* and *rin* alters the overall RpL/RpS stoichiometry. Treatment with sulfaquinoxaline and apigenin induces readthrough of eukaryotic translation, leading to RQC, synthesis of a truncated polypeptide chain, and subsequent ubiquitination of RpS subunits. (2A,B) We found that overexpression of *Usp10* and *rin* reduces the toxicity of apigenin and sulfoquinoxinaline and effectively eliminates ubiquitination on the RpS subunits. In contrast, RNAi flies were more sensitive to ribotoxicity triggered by translational readthrough, as shown by shortened lifespan and enhanced ubiquitination of RpS subunits.

Discussion

  This work represents findings related to Foozhan's project linking the 40S subunit to mitochondrial morphology and energy dynamics. Protein translation is a major consumer of ATP in the cell. Protein translation and mitochondrial dysfunction exist in a feedback loop, wherein a loss of mitochondrial function may affect protein translation and ribosomal stalling, and a loss of quality control of protein translation can have direct effects on mitochondrial function.[42]

  Sulfaquinoxaline and apigenin may chemically replicate times of cellular stress and mRNA strands that have damaged or premature stop codons. To establish a connection between proteostatic stress and mitochondrial dysfunction, we confirmed that the RQC mechanisms of Usp10 and *rin* do indeed play an essential role in preventing chemically induced protein toxicity.
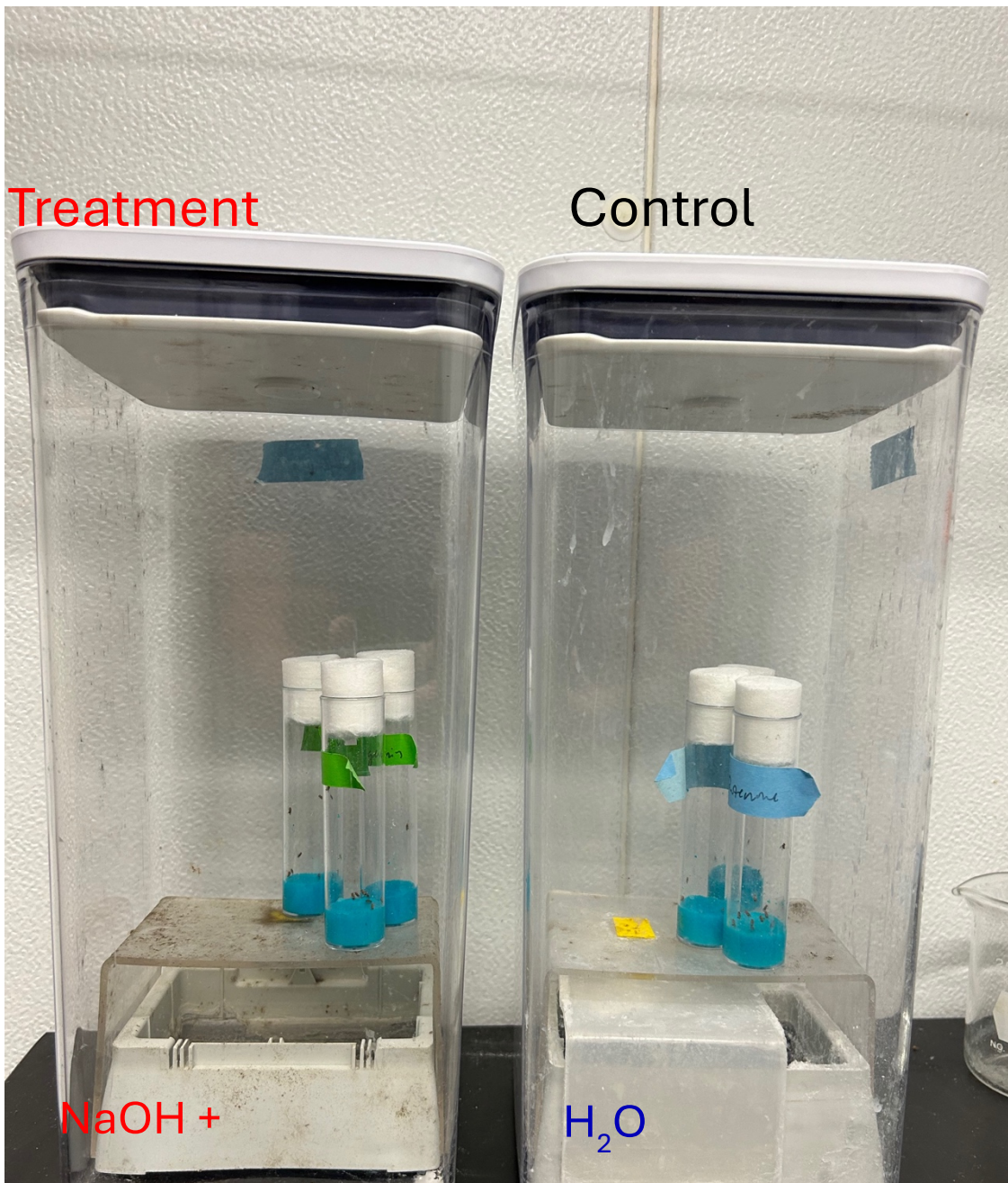
Supplementary Figure 1 Method for Hydrogen Treatment

Supplementary Materials

Fly Stocks Used				
First Appearance	**Gene Name**	**ID** Table 1 Drosophila Genotype Information.48	**Full Genotype**	**Notes**
Figure 2	w1118	RRID:BDSC_5905	w[1118]	N/A
Figure 3	TDP-43.A315T	GC01P039670	UAS-TDP43.A315T[A10] / TM3,sb	Courtesey of Jane Wu lab at Northwestern University
Figure 3	P525L.FUS	GC16P031180	UAS-P525L.FUS.RFP[PR8a] / MRS	Courtesey of Jane Wu lab at Northwestern University
figure 3	GR80	N/A	UAS-FLAG.GR80 (III)	Courtesey of Fen-Biao Gao lab at University of Massachusetts
Figure 4	TDP-43 WT	GC01P039671	UAS-TDP43.WT.RFP / TM6	Courtesey of Jane Wu lab at Northwestern University
Figure 4	RFP(control)	N/A	UAS-RFP / CyO (control)	Courtesey of Jane Wu lab at Northwestern University
Figure 4	FUS WT	GC16P031181	UAS-FUS.RFP; FRK/CyO (X)	Courtesey of Jane Wu lab at Northwestern University
figure 5	dPink1 RNAi	CG4523	MH-Gal4>UAS-Pink1 RNAi#6 (III)	N/A
figure 5	mitoGFP	N/A	MHC>mitoGFP / TM2	N/A
figure 6	B9: Pink1[B9] mutant (KO)	CG4524	B9 / FM6; ; MHC> mitoGFP / TM2	N/A
Figure 8	Usp10 RNAi	CG32479	Usp10 RNAi-GD (III)	Courtesey of Shian Wu lab at NanKai University
Figure 8	rin RNAi	CG9412	Rin(CG9412) RNAi KK (II)	N/A

Table 1 Drosophila Genotype Information

REAGENT or RESOURCE	SOURCE	IDENTIFIER
Antibodies		
Chicken anti-GFP	Abcam	ab13970
Rabbit anti-ref(2)P	Abcam	Ab177440
Goat anti-Chicken IgY (H+L) Secondary Antibody, Alexa Fluor 488	Invitrogen	A11039
Goat anti-Mouse IgG (H+L) Highly Cross-Adsorbed Secondary Antibody, Alexa Fluor 488	Invitrogen	A32732
Goat anti-Rabbit IgG (H+L) Highly Cross-Adsorbed Secondary Antibody, Alexa Fluor 568	Invitrogen	A11036
Goat anti-Mouse IgG (H+L) Cross-Adsorbed Secondary Antibody, Alexa Fluor 568	Invitrogen	A11004
Goat anti-Rabbit IgG (H+L) Cross-Adsorbed Secondary Antibody, Alexa Fluor 633	Invitrogen	A21071
Goat anti-Mouse IgG (H+L) Cross-Adsorbed Secondary Antibody, Alexa Fluor 633	Invitrogen	A21050
Goat anti-rabbit HRP	Invitrogen	G21234
Goat anti-mouse HRP	Invitrogen	PI31430
Chemicals, kits, and critical commercial assays		
Hydrogen container	OXO	amazon.com
10 M Sodium Hydroxide Solution	Fischer Scientific	1310-73-2
Aluminum	Reynolds Wrap	Amazon.com
Instant *Drosophila* medium	Carolina	FAM_173210
DAPI	Fisher Scientific	57-481-0
Software and Algorithms		
BioRender	BioRender	https://biorender.com/
GraphPad Prism 9.4. 1	GraphPad	https://www.graphpad.com/scientific-software/prism/
ImageJ 1.53t	National Institute of Health	https://imagej.nih.gov/ij/download.html
ImageJ plug in: Mitochondria-Analyzer	Ahsen Chaudhry	https://github.com/AhsenChaudhry/Mitochondria-Analyzer
ZEN (blue edition)	ZEISS	https://www.zeiss.com/microscopy/us/products/microscope-software.html

Table 2 Reagents or Resources

BIBLIOGRAPHY

1. Saikumar, J. *et al.* Inducing different severities of traumatic brain injury in Drosophila using a piezoelectric actuator. *Nat. Protoc.* **16**, 263–282 (2021).

2. Maas, A. I. R. *et al.* Traumatic brain injury: integrated approaches to improve prevention, clinical care, and research. *Lancet Neurol.* **16**, 987–1048 (2017).

3. Saikumar, J., Byrns, C. N., Hemphill, M., Meaney, D. F. & Bonini, N. M. Dynamic neural and glial responses of a head-specific model for traumatic brain injury in Drosophila. *Proc. Natl. Acad. Sci.* **117**, 17269–17277 (2020).

4. Mez, J. *et al.* Clinicopathological Evaluation of Chronic Traumatic Encephalopathy in Players of American Football. *JAMA* **318**, 360–370 (2017).

5. Chodobski, A., Zink, B. J. & Szmydynger-Chodobska, J. Blood-brain barrier pathophysiology in traumatic brain injury. *Transl. Stroke Res.* **2**, 492–516 (2011).

6. Aggarwal, P., Thapliyal, D. & Sarkar, S. The past and present of Drosophila models of traumatic brain injury. *J. Neurosci. Methods* **371**, 109533 (2022).

7. Daneshvar, D. H., Goldstein, L. E., Kiernan, P. T., Stein, T. D. & McKee, A. C. Post-traumatic neurodegeneration and chronic traumatic encephalopathy. *Mol. Cell. Neurosci.* **66**, 81–90 (2015).

8. Johnson, V. E., Stewart, W. & Smith, D. H. Traumatic brain injury and amyloid-β pathology: a link to Alzheimer's disease? *Nat. Rev. Neurosci.* **11**, 361–370 (2010).

9. Traumatic Brain Injury and Neuropsychiatric Complications - Saeed Ahmed, Hema Venigalla, Hema Madhuri Mekala, Sara Dar, Mudasar Hassan, Shahana Ayub, 2017. https://journals.sagepub.com/doi/10.4103/0253-7176.203129.

10. McGurk, L., Berson, A. & Bonini, N. M. Drosophila as an In Vivo Model for Human Neurodegenerative Disease. *Genetics* **201**, 377–402 (2015).

11. Anderson, E. N. *et al.* Traumatic injury induces stress granule formation and enhances motor dysfunctions in ALS/FTD models. *Hum. Mol. Genet.* **27**, 1366–1381 (2018).

12. Sorrentino, V., Menzies, K. J. & Auwerx, J. Repairing Mitochondrial Dysfunction in Disease. *Annu. Rev. Pharmacol. Toxicol.* **58**, 353–389 (2018).

13. Mitchell, P. Chemiosmotic coupling in oxidative and photosynthetic phosphorylation. *Biochim. Biophys. Acta BBA - Bioenerg.* **1807**, 1507–1538 (2011).

14. Devine, M. J. & Kittler, J. T. Mitochondria at the neuronal presynapse in health and disease. *Nat. Rev. Neurosci.* **19**, 63–80 (2018).

15. Llanos-González, E. *et al.* Interplay Between Mitochondrial Oxidative Disorders and Proteostasis in Alzheimer's Disease. *Front. Neurosci.* **13**, 1444 (2020).

16. de Boer, E. M. J. *et al.* TDP-43 proteinopathies: a new wave of neurodegenerative diseases. *J. Neurol. Neurosurg. Psychiatry* **92**, 86–95 (2021).

17. Barmada, S. J. *et al.* Cytoplasmic Mislocalization of TDP-43 Is Toxic to Neurons and Enhanced by a Mutation Associated with Familial Amyotrophic Lateral Sclerosis. *J. Neurosci.* **30**, 639–649 (2010).

18. Neumann, M. *et al.* Ubiquitinated TDP-43 in frontotemporal lobar degeneration and amyotrophic lateral sclerosis. *Science* **314**, 130–133 (2006).

19. Ling, J. P., Pletnikova, O., Troncoso, J. C. & Wong, P. C. TDP-43 repression of nonconserved cryptic exons is compromised in ALS-FTD. *Science* **349**, 650–655 (2015).

20. Tank, E. M. *et al.* Abnormal RNA stability in amyotrophic lateral sclerosis. *Nat. Commun.* **9**, 2845 (2018).

21. Colantoni, A. *et al.* FUS Alters circRNA Metabolism in Human Motor Neurons Carrying the ALS-Linked P525L Mutation. *Int. J. Mol. Sci.* **24**, 3181 (2023).

22. Honda, H. *et al.* Mutated FUS in familial amyotrophic lateral sclerosis involves multiple hnRNPs in the formation of neuronal cytoplasmic inclusions. *J. Neuropathol. Exp. Neurol.* **82**, 231–241 (2023).

23. Ho, W. Y. *et al.* Dysfunction in nonsense-mediated decay, protein homeostasis, mitochondrial function, and brain connectivity in ALS-FUS mice with cognitive deficits. *Acta Neuropathol. Commun.* **9**, 9 (2021).

24. Balendra, R. & Isaacs, A. M. C9orf72-mediated ALS and FTD: multiple pathways to disease. *Nat. Rev. Neurol.* **14**, 544–558 (2018).

25. Gendron, T. F. & Petrucelli, L. Disease Mechanisms of C9ORF72 Repeat Expansions. *Cold Spring Harb. Perspect. Med.* **8**, a024224 (2018).

26. Li, S. *et al.* Quality-control mechanisms targeting translationally stalled and C-terminally extended poly(GR) associated with ALS/FTD. *Proc. Natl. Acad. Sci. U. S. A.* **117**, 25104–25115 (2020).

27. Yu, C.-H. *et al.* TDP-43 Triggers Mitochondrial DNA Release via mPTP to Activate cGAS/STING in ALS. *Cell* **183**, 636-649.e18 (2020).

28. Thammisetty, S. S. *et al.* Age-related deregulation of TDP-43 after stroke enhances NF-κB-mediated inflammation and neuronal damage. *J. Neuroinflammation* **15**, 312 (2018).

29. Picard, M. & Turnbull, D. M. Linking the Metabolic State and Mitochondrial DNA in Chronic Disease, Health, and Aging. *Diabetes* **62**, 672–678 (2013).

30. Ježek, J., Cooper, K. F. & Strich, R. Reactive Oxygen Species and Mitochondrial Dynamics: The Yin and Yang of Mitochondrial Dysfunction and Cancer Progression. *Antioxidants* **7**, 13 (2018).

31. Chaudhry, A., Shi, R. & Luciani, D. S. A pipeline for multidimensional confocal analysis of mitochondrial morphology, function, and dynamics in pancreatic β-cells. *Am. J. Physiol.-Endocrinol. Metab.* **318**, E87–E101 (2020).

32. Yang, Y. *et al.* Pink1 regulates mitochondrial dynamics through interaction with the fission/fusion machinery. *Proc. Natl. Acad. Sci.* **105**, 7070–7075 (2008).
33. Narendra, D. P. *et al.* PINK1 Is Selectively Stabilized on Impaired Mitochondria to Activate Parkin. *PLOS Biol.* **8**, e1000298 (2010).